SUMOylation Restricts Adaptive Thermogenesis by Suppressing Beiging Gene Networks

by

Patrizia Nothnagel [a], Nolwenn Briand [b], Jonas Aakre Wik [c], Yunna E. Strøm [a,l], Magnar Bjørås [d,e,f], Jorrit M. Enserink [a,g,h], Bjørn Steen Skålhegg [c], Anthony Mathelier [i,j,k] and Pierre Chymkowitch [a,*]

[a] Department of Biosciences, Faculty of Mathematics and Natural Sciences, University of Oslo, 0316, Oslo, Norway.

[b] Department of Molecular Medicine, Faculty of Medicine, Institute of Basic Medical Sciences, University of Oslo, Blindern, PO Box 1112, 0317, Oslo, Norway.

[c] Division for Molecular Nutrition, Institute of Basic Medical Sciences, University of Oslo, Oslo, Norway.

[d] Department of Clinical and Molecular Medicine, Norwegian University of Science and Technology, 7491, Trondheim, Norway.

[e] Department of Microbiology, Oslo University Hospital, Oslo, Norway

[f] Centre for Embryology and Healthy Development (CRESCO), University of Oslo, Oslo, 0373, Norway.

[g] Department of Molecular Cell Biology, Institute for Cancer Research, Oslo University Hospital, 0372, Oslo, Norway.

[h] Centre for Cancer Cell Reprogramming, Institute of Clinical Medicine, Faculty of Medicine, University of Oslo, 0318, Oslo, Norway.

[i] Centre for Molecular Medicine Norway (NCMM), Nordic EMBL Partnership, University of Oslo, Oslo 0318, Norway.

[j] Department of Medical Genetics, Institute of Clinical Medicine, Oslo University Hospital and University of Oslo, Oslo, Norway.

[k] Department of Pharmacy, University of Oslo, Oslo, Norway.

[1] Present address: Department of Molecular Biology, Faculty of Science, Radboud Institute for Molecular Life Sciences, Oncode Institute, Radboud University Nijmegen, 6525 GA Nijmegen, The Netherlands

* Corresponding author

Abstract

Adaptive thermogenesis, or beiging, involves the conversion of energy-storing white adipocytes into energy-dissipating beige adipocytes, enabling physiological adaptation to environmental stressors such as hypothermia. While white and beige adipocytes share transcriptional similarity, this identity switch still requires transcriptional and epigenetic reprogramming. However, the molecular mechanisms governing this transition remain incompletely understood. Here, we identify SUMOylation as a critical repressor of adipocyte beiging. Using the small-molecule SUMOylation inhibitor TAK-981, we demonstrate that transient inhibition of SUMOylation primes human adipocytes to express beiging genes including *UCP1* and inducing mitochondrial uncoupling in a rosiglitazone-dependent manner. Furthermore, SUMOylation suppresses both the *de novo* differentiation of human adipose stem cells into beige adipocytes and the transdifferentiation of mature white adipocytes into beige cells. Mechanistically, TAK-981 modulates the cAMP-PKA-p38 signaling axis, ultimately affecting downstream transcriptional programs under the control of PPARG and PPARA enhancers. Our findings establish SUMOylation as a fundamental barrier to white-to-beige adipocyte reprogramming and suggest that the pharmacological combination of PPARG agonists with TAK-981 can promote metabolically beneficial adipose tissue remodeling in clinical settings.

Introduction

Post-translational modification by the small ubiquitin-like modifier (SUMO) constitutes a reversible process in which a SUMO peptide is covalently conjugated to target proteins, thereby modulating their function, localization, and stability (Chymkowitch *et al*, 2015b). Over the past decade, extensive research has elucidated the critical role of the SUMOylation pathway in cellular differentiation and development, employing diverse in vitro and in vivo models (Cossec *et al*, 2018; Cossec *et al*, 2023; Dufour *et al*, 2022; Zhao *et al*, 2022). Although the precise molecular mechanisms underlying SUMOylation and its substrate specificity remain incompletely defined, accumulating evidence underscores its indispensability in developmental processes and its involvement in nearly all cellular functions — particularly nuclear events. Notably, a dynamic equilibrium between SUMOylation and deSUMOylation is fundamental for the formation and functional maturation of multiple cell types and organs, including adipose tissue (Antonio Urrutia *et al*, 2021; Chung *et al*, 2010; Cignarelli *et al*, 2010; Cox *et al*, 2021; Demarque *et al*, 2011; Dufour *et al.*, 2022; Liu *et al*, 2014; Mikkonen *et al*, 2013; Pei *et al*, 2024; Zhao *et al.*, 2022; Zheng *et al*, 2018).

Crucially, SUMOylation has been implicated in the repression of cellular reprogramming through modification of key regulators of chromatin architecture, epigenetic landscapes, and transcriptional activity (Boulanger *et al*, 2021; Cossec *et al.*, 2018; Cossec *et al.*, 2023; Rosonina *et al*, 2017; Zhao *et al.*, 2022). These findings highlight the essential role of SUMOylation in maintaining epigenetic integrity and cellular homeostasis. Unsurprisingly, dysregulation of this pathway has been linked to pathological conditions, including oncogenesis (Seeler & Dejean, 2017).

Adipogenesis is an excellent model system for studying the role of SUMOylation in epigenetic memory and cellular reprogramming. Notably, the formation and functional maturation of white adipose tissue (WAT) appear to be critically dependent on a dynamic SUMOylation/deSUMOylation cycle, which orchestrates gene expression and repression programs essential for adipogenic differentiation (Cignarelli *et al.*, 2010; Cox *et al.*, 2021; Zhao *et al.*, 2022). WAT plays a central role in energy homeostasis by regulating lipid storage and mobilization in response to metabolic demands. Under conditions of positive energy balance, WAT sequesters excess lipids to prevent lipotoxicity and associated metabolic complications, such as hepatic steatosis. Conversely, during energy deficit, WAT undergoes lipolysis, releasing fatty acids as an alternative energy source to maintain systemic energy balance.

Remarkably, WAT exhibits plasticity and undergoes phenotypic conversions in response to environmental stimuli such as cold exposure. This process, termed adaptive thermogenesis or "beiging," is characterized by the emergence of beige adipocytes within WAT (Rosenwald & Wolfrum, 2014; Shapira & Seale, 2019). Unlike classical white adipocytes, which primarily function as lipid storage depots, beige adipocytes possess the capacity to oxidize fatty acids and utilize oxygen to generate heat through uncoupling of the mitochondrial respiratory chain, a process mediated by uncoupling protein 1 (UCP1) (Chang *et al*, 2019).

Although white and beige adipocytes exhibit largely overlapping gene expression profiles (Christy *et al*, 1991; Clarke *et al*, 1997; Farmer, 2006; Lee *et al*, 2003), beige adipocytes uniquely express genes associated with mitochondrial uncoupling and energy dissipation, including *UCP1* (Shapira & Seale, 2019). Evidence suggests that beiging occurs through the transdifferentiation of mature white adipocytes into beige adipocytes in response to hypothermic conditions, a process that is reversible in a temperature dependent fashion

(Rosenwald *et al*, 2013). Transcriptomic analyses further support this model, revealing that a subset of white adipocytes is transcriptionally primed for beige conversion (Rosenwald & Wolfrum, 2014). In addition to transdifferentiation, beige adipocytes may arise from distinct progenitor populations or via the reprogramming of differentiating white adipocytes (Merrick *et al*, 2019; Schwalie *et al*, 2018). However, the molecular mechanisms governing the induction or suppression of white-to-beige gene expression programs and associated epigenetic remodeling remain largely unresolved. Elucidating these mechanisms may provide critical insight into the regulation of adaptive thermogenesis and offer novel therapeutic strategies for combating obesity (Pahlavani *et al*, 2024).

Globally, obesity and its related conditions, including type 2 diabetes, now cause more deaths than starvation (The Lancet, Global Burden of Disease)[1]. Strong evidence links obesity to a higher risk of several cancers (Liu *et al*, 2021; Nguyen *et al*, 2023; Nordsletten *et al*, 2023; Pati *et al*, 2023) and severe SARS-CoV-2 infection, with severity correlating with body mass index (Kalligeros *et al*, 2020). Current treatments—diets, medications, exercise, surgery, and liposuction—often fail to restore metabolic balance or sustain weight loss, possibly due to an epigenetic obesogenic memory (Chang *et al.*, 2019; Hinte *et al*, 2024). This highlights the need for new, non-invasive therapies. Understanding WAT "beiging" and its role in energy expenditure could offer promising strategies to combat obesity and its complications (Hanssen *et al*, 2015; Pahlavani *et al.*, 2024; Shapira & Seale, 2019).

Given its established role in maintaining cellular identity, we hypothesized that SUMOylation may play a regulatory role in limiting the plasticity of white adipose tissue (WAT), specifically the transcriptional and metabolic reprogramming associated with the conversion of white adipocytes to beige adipocytes. In this study, we demonstrate that

[1] Global Burden of Disease Collaborative Network. Global Burden of Disease Study 2021 (GBD 2021). Seattle, United States: Institute for Health Metrics and Evaluation (IHME), 2024.

transient inhibition of SUMOylation using TAK-981 in both human adipose stem cells (hASCs) and mature adipocytes is sufficient to induce a stable white-to-beige adipocyte transition. This conversion is accompanied by mitochondrial uncoupling and increased energy expenditure, a process that is dependent on the antidiabetic drug rosiglitazone.

Results

Transient SUMOylation inhibition primes hASCs to express UCP1.

To investigate the role of SUMOylation in adipocyte beiging, we transiently treated human adipose stem cells (hASCs) (Xue *et al*, 2015) with TAK-981, a selective inhibitor of the SUMOylation pathway currently in clinical trials as a potential cancer therapy (Dudek *et al*, 2021; Langston *et al*, 2021) (Fig. 1A). In parallel, cells were treated with rosiglitazone, a peroxisome proliferator-activated receptor gamma (PPARG) agonist and well-established inducer of adipocyte beiging (Ohno *et al*, 2012). This rosiglitazone treatment excided in time the regular short treatment necessary to achieve adipogenesis. Finally, a third experimental condition combined TAK-981 with rosiglitazone to assess potential synergistic effects.

Western blot analysis for SUMO-2/3 confirmed the transient nature of SUMOylation inhibition, as SUMOylation levels recovered within two days following TAK-981 treatment. This analysis also revealed that rosiglitazone treatment did not have a noticeable effect on global SUMOylation levels (Fig. 1B). To evaluate the impact of these treatments on adipocyte differentiation, we performed Oil-Red-O staining at different time points after SUMOylation recovery (days 22 and 32, Suppl. Fig. S1A). As expected, rosiglitazone treatment enhanced lipid accumulation compared to control cells (Suppl. Fig. S1A) (Ohno *et al.*, 2012). Notably, a similar increase in lipid accumulation was observed following TAK-981 treatment, suggesting that SUMOylation inhibition promotes adipogenesis in hASCs, consistent with our previous findings (Bjune et al., 2023). However, the combination of

TAK-981 and rosiglitazone did not further enhance adipogenesis beyond the effects observed with individual treatments (Suppl. Fig. S1A).

We next examined the effects of these treatments on the expression of adipogenic genes using RT-qPCR. Both rosiglitazone and TAK-981 significantly upregulated *PPARG* expression compared to control cells (Fig. 1C). However, co-treatment with both molecules did not further enhance *PPARG* expression beyond the levels observed with either treatment alone (Fig. 1C). A similar trend or an additive effect was observed for other adipogenic markers (Suppl. Fig. S1B), consistent with the increased lipid accumulation observed in Suppl. Figure S1A.

To assess the impact of SUMOylation inhibition on adipocyte beiging, we quantified the expression of *UCP1*, a hallmark of white-to-beige adipocyte conversion and a key mediator of mitochondrial uncoupling (Chang *et al.*, 2019). Notably, while *UCP1* expression was undetectable in control cells and, as expected, only weakly induced by either rosiglitazone or TAK-981 alone, co-treatment with both molecules led to a striking and synergistic increase in *UCP1* expression (Fig. 1D).

To determine whether the observed increase in *UCP1* mRNA levels correlated with enhanced UCP1 protein expression, we performed western blot analysis using differentiated brown adipocytes as a positive control (Xue *et al.*, 2015). Consistent with *UCP1* transcript levels (Fig. 1D) and previous studies (Ohno *et al.*, 2012), UCP1 protein expression was only weakly detectable at day 32 in cells treated with rosiglitazone alone (Fig. 1E). A faint UCP1 band was also observed in TAK-981-treated cells at day 32 (Fig. 1E). In contrast, co-treatment with TAK-981 and rosiglitazone resulted in a robust increase in UCP1 protein levels, which became evident as early as day 22 and which reflected the dynamics of *UCP1* mRNA levels (Fig. 1D, E).

Together, these data indicate that transient inhibition of SUMOylation in human adipose stem cells, prior to adipogenic induction, primes the cells to respond faster and stronger to rosiglitazone to unleash the expression of *UCP1*.

Transient SUMOylation inhibition in mature adipocytes leads to UCP1 expression.

To determine whether inhibition of SUMOylation can also induce beiging of mature adipocytes, we transiently treated fully differentiated adipocytes with TAK-981 in the presence or absence of rosiglitazone (Fig. 2A). Western blot analysis for SUMO-2/3 confirmed the transient nature of SUMOylation inhibition (Fig. 2B). To assess the impact of these treatments on lipid accumulation, we performed Oil-Red-O staining at multiple time points following SUMOylation recovery (Days 22, 27 and 32). As observed in pre-adipocytes (Suppl. Fig. S1A), rosiglitazone progressively enhanced lipid accumulation relative to control cells (Suppl. Fig. S1C). However, in contrast to pre-adipocytes, TAK-981 treatment alone had no detectable effect on adipogenesis in mature adipocytes (Suppl. Fig. S1C). The combination of TAK-981 and rosiglitazone moderately enhanced fat accumulation beyond the levels observed with rosiglitazone alone (Suppl. Fig. S1C). Note that such an enhanced fat accumulation has been show to cooccur with beiging (Ellis *et al*, 2010; Guilherme *et al*, 2020a). In this experimental setting, TAK-981 treatment did not significantly affect *PPARG* expression (Fig. 2C, D). Similarly, rosiglitazone alone had no significant effect on *PPARG* expression until day 21 (Fig. 2C), although at later time points its expression increased significantly (Fig. 2D). Notably, co-treatment with TAK-981 and rosiglitazone resulted in an additive increase in *PPARG* expression (Fig. 2C, D). A similar trend was observed for other adipogenic markers (Suppl. Fig. S1D).

Next, we assessed *UCP1* expression. Compared to what we observed in adipose stem cells, in mature adipocytes *UCP1* transcript levels remained very low in control, TAK-981-,

and rosiglitazone-treated cells until day 21 (Fig. 2E). However, at later time points (days 27–32), TAK-981 and rosiglitazone synergistically promoted a marked upregulation of *UCP1* expression (Fig. 2F).

To further investigate the impact of SUMOylation inhibition on adipocyte beiging, we analyzed UCP1 protein levels across multiple time points. UCP1 was undetectable in control cells and in cells treated with TAK-981 alone (Fig. 2G), whereas rosiglitazone treatment led to a progressive increase in UCP1 protein levels over time (Fig. 2G), in agreement with *UCP1* mRNA expression (Fig. 2F) and a previous report (Ohno *et al.*, 2012). However, as observed in pre-adipocytes (Fig. 1E), co-treatment with TAK-981 and rosiglitazone resulted in a marked increase of UCP1 protein levels (Fig. 2G).

Collectively, these findings (Figure 1 and 2) indicate that a combination of rosiglitazone with transient inhibition of SUMOylation results in reprogramming of hASCs and mature white adipocytes into beige adipocytes (Fig. 2H).

UCP1 **derepression leads to mitochondrial uncoupling**

Transition of white into beige adipocytes, i.e. expression of UCP1, is expected to enhance mitochondrial uncoupling, leading to increased oxidative metabolism and energy expenditure. To directly assess this, we measured the oxygen consumption rate (OCR) and extracellular acidification rate (ECAR) at day 22 in cells subjected to the treatments described in Fig. 1A (Fig. 3A), using brown adipocytes as a positive control. Consistent with the observed UCP1 upregulation, co-treatment with TAK-981 and rosiglitazone resulted in a significant increase in OCR, even exceeding the levels observed in brown adipocytes (Fig. 3B), whereas ECAR was elevated to levels comparable to those of brown adipocytes (Fig. 3C). Integrating OCR and ECAR data revealed a pronounced shift toward a highly energetic

metabolic state in TAK-981 and rosiglitazone-treated cells, resembling the metabolic profile of brown adipocytes (Fig. 3D).

To determine whether similar metabolic reprogramming occurs in mature adipocytes, we performed the same experiments at day 32 in cells subjected to the treatments described in Fig. 2A (Fig. 3E). Again, cells co-treated with TAK-981 and rosiglitazone exhibited a significant increase in both OCR and ECAR (Fig. 3F, G) along with enhanced mitochondrial uncoupling (Fig. 3H), further supporting a metabolic shift toward beiging.

Collectively, these data demonstrate that TAK-981 and rosiglitazone synergize to induce stable beiging of white adipocytes. These findings also indicate that SUMOylation functions as a repressive mechanism that limits both the reprogramming of human adipose stem cells and the transdifferentiation of mature white adipocytes into beige adipocytes.

TAK-981 steers the transcriptome of white adipocytes towards beiging in a rosiglitazone-dependent manner

To elucidate the transcriptional reprogramming triggered by TAK-981 and rosiglitazone, we performed RNA sequencing (RNA-seq) at day 21 in cells subjected to the treatments described in Fig. 1A. Differentially expressed gene (DEG) analysis ($\log\square FC > 1$ or $\log\square FC < -1$; $padj < 0.05$) revealed significant transcriptomic alterations in all three conditions compared to control cells (Fig. 4A–F). TAK-981 alone led to 336 downregulated and 1,169 upregulated genes (Suppl. Table S1, Fig. 4A), which is consistent with previous reports indicating that SUMOylation functions as both a transcriptional repressor and activator, with a predominant role in gene repression (Baig *et al*, 2021; Chymkowitch *et al*, 2015a; Chymkowitch *et al*, 2017; Launonen *et al*, 2024; Nguea *et al*, 2019; Zhao *et al.*, 2022). Rosiglitazone alone resulted in 524 downregulated and 960 upregulated genes (Suppl. Table S1, Fig. 4B), while co-treatment with TAK-981 and rosiglitazone induced the most

extensive transcriptomic changes, with 953 downregulated and 2,064 upregulated genes (Suppl. Table S1, Fig. 4C).

Gene ontology (GO) analysis of biological processes revealed a strong enrichment for fatty acid metabolic pathways across all three conditions (Fig. 4D-F; Suppl. Table S2), which aligns with the established role of lipid metabolism in both white and beige adipocytes (Guilherme *et al*, 2020b). Notably, despite significant transcriptional alterations, none of the treatments alone or in combination resulted in a definitive beiging-specific transcriptional signature.

We then compared TAK-981 + rosiglitazone to rosiglitazone alone, using the latter as a baseline to uncover genes whose regulation was specifically enhanced by SUMOylation inhibition. We identified 682 upregulated and 190 downregulated genes (DEG; $\log\square FC > 1$ or $\log\square FC < -1$; padj < 0.05) (Suppl. Table S1, Fig. 5A). Importantly, GO analysis of upregulated genes revealed a significant enrichment for brown/beige adipocyte-related processes, including adaptive thermogenesis and temperature homeostasis (Fig. 5B, Suppl. Table S2). Closer examination of these DEGs confirmed that inhibition of SUMOylation amplified the expression of key beiging markers, such as *ELOVL3*, *CIDEA*, and *UCP1* (Fig. 5A-C; Suppl. Table S2). In contrast, downregulated genes were not associated with adipogenesis or adaptive thermogenesis, suggesting that SUMOylation inhibition selectively reinforces beiging rather than disrupting general functions of adipocytes (Fig. 5D; Suppl. Table S2).

Together, these findings indicate that SUMO serves as a barrier to prevent transcriptional reprogramming toward a beige adipocyte identity.

Inhibition of SUMOylation enhances cAMP-PKA-p38 signaling to facilitate beiging

To investigate the molecular basis of the transcriptional remodeling observed above, we examined the activation of the cAMP-PKA-p38 signaling axis, a key pathway in adaptive thermogenesis. During adaptive thermogenesis, this pathway is initiated by β3-adrenergic receptor (β3-AR) activation, leading to PKA-dependent phosphorylation of nuclear substrates (e.g., CREB, JMJD1A) that drive beiging gene expression (e.g., *UCP1*, *PPARGC1A*, *PPARG*) (Guilherme *et al.*, 2020b). PKA also phosphorylates cytoplasmic targets such as PLIN1 and HSL, facilitating lipolysis and activating p38, which in turn phosphorylates ATF2 to derepress *UCP1* expression (Fig. 6A and Suppl. Fig. S2A) (Cao *et al*, 2004; Inagaki *et al*, 2016).

We hypothesized that inhibition of SUMOylation enhances cAMP-PKA-p38 signaling. Interestingly, KEGG pathway enrichment analysis revealed that TAK-981 + rosiglitazone treatment, compared to rosiglitazone alone, resulted in significantly increased expression of genes involved in the pathway "adaptive thermogenesis" including components of cAMP-PKA-p38 signaling, such as *Gs*, adenylate cyclase subunits, *JMJD1A*, *PPARGC1A*, and *PPARG* (Fig. 6B and Suppl. Fig. S2A). In contrast, we observed reduced expression of *CB1R*, a known adenylate cyclase inhibitor, suggesting further contribution to sustained PKA activation (Fig. 6B and Suppl. Fig. S2A). Furthermore, downstream genes involved in thermogenesis, such as lipolysis-associated genes (*PLIN1*, *PNPLA2*, *LIPE*) were also upregulated, further supporting beiging activation. Finally, expression of genes encoding OXPHOS components was also significantly increased, correlating with the high-energy metabolic state of TAK-981 + rosiglitazone-treated cells (Fig. 3A–F, Fig. 5B and Suppl. Fig. S3A). These data indicate that the thermogenesis pathway was activated in TAK-981 + rosiglitazone-treated cells, starting with cAMP-PKA-p38 signaling activation, which led to *UCP1* and OXPHOS genes induction.

To more directly assess whether these transcriptional changes translated into enhanced pathway activity, we examined the phosphorylation of PKA and p38 substrates. Western blot analysis using a pan-PKA phospho-specific substrate antibody showed that TAK-981 alone was a stronger activator of PKA than rosiglitazone for certain targets. Combining the two drugs yielded a more significant activation of PKA than observed with Rosiglitazone alone but not with TAK-981 alone (Fig. 6C and D). Specific analysis of CREB phosphorylation confirmed that TAK-981 and rosiglitazone each enhanced CREB phosphorylation, but their combination yielded an additional increase in CREB phosphorylation (Fig. 6E and F). Notably, ATF-1 phosphorylation followed a similar pattern, further supporting enhanced PKA signaling (Fig. 6E). p38 phosphorylation was also significantly increased by both TAK-981 and rosiglitazone, although there was no additional effect of their combination (Fig. 6E and G). However, phosphorylation of p38's thermogenic target, ATF2, was significantly stronger when both drugs were combined (Fig. 6E and H).

Together, these findings suggest that SUMOylation restricts beiging via two non-exclusive mechanisms: 1) Transcriptional repression of key components in the cAMP-PKA-p38 pathway, as well as genes encoding downstream OXPHOS proteins; 2) Direct negative regulation of PKA and p38 kinase activities, limiting their capacity to drive thermogenic gene expression.

Sumoylation inhibition enhances PPARA/PPARG activation and epigenetic remodeling to drive beiging

To further characterize the impact of SUMOylation inhibition on adaptive thermogenesis, we sought to identify gene regulators acting downstream of the cAMP-PKA-p38 axis that mediate the transcriptional switch to beiging (Fig. 5 and Fig. 7A) (Badia *et al*, 2022; Turei *et al*, 2021). Our analysis predicted that SREBP1, PPARA, and PPARG were the

primary TFs mobilized upon SUMOylation inhibition (Fig. 7B). Consistently, beiging genes such as *SLC2A4* (GLUT4), *LEP* (Leptin) and *UCP1*, were induced by PPARA and PPARG, *ACSL1* (Acyl-CoA Synthetase) by PPARA and *ADIPOR2* (Adiponectin receptor) by PPARG upon transient SUMOylation inhibition (Fig. 7C and D). These findings suggest that upregulation of the cAMP-PKA-p38 pathway led to PPARA/G activation, as expected during beiging (Suppl. Fig. S2A). Alternatively, SUMOylation inhibition may directly impact PPARA and PPARG transactivation activity, given that both are well-characterized SUMO targets, and SUMOylation can either enhance or repress their function (Boulanger *et al.*, 2021; Hendriks *et al*, 2018; Katafuchi *et al*, 2018; Zhao *et al.*, 2022) (Fig. 7A). Based on this, and since *UCP1* is not a direct target of SREBP1 (Suppl. Fig. S2B), we focused our attention on PPARA and PPARG activation.

To validate the activation of PPARA and PPARG in response to TAK-981, we measured the activity of PPAR response elements (PPREs) linked to key beiging genes: *TSHR*, *ACSL1*, *UCP1*, *PGC1A*, and *CIDEA* (Fig. 7E-I). These PPREs were primarily identified using the JASPAR database (Rauluseviciute *et al*, 2024). To assess PPRE activity, we performed ChIP-qPCR for the occurrence of H3K27ac (active enhancers) and H3K27me3 (repressed enhancers). These experiments showed that treatment with either rosiglitazone or TAK-981 alone led to a significant increase in the occurrence of H3K27ac at *TSHR* and *ACSL1* PPREs (Fig. 7J, left). At the same time, we observed a decrease in H3K27me3, which was particularly evident at ^{PPRE1}*TSHR* and ^{PPRE}*ACSL1* (Fig. 7K, left). Importantly, when rosiglitazone and TAK-981 were combined, the increase in H3K27ac levels became more pronounced at these PPREs, while the presence of H3K27me3 decreased significantly (Fig. 7J and K, left). These findings align with our expression data (Fig. 4A and Fig. 7C and D) and support a previous observation that *TSH1* expression is directly linked to *UCP1* activation during adaptive thermogenesis (Guilherme *et al.*, 2020b).

When examining *UCP1* PPREs, we found that TAK-981 treatment alone resulted in a strong and significant increase in H3K27ac, accompanied by a decrease in H3K27me3. However, rosiglitazone alone had no effect on these marks, and co-treatment with rosiglitazone and TAK-981 did not further alter them when compared to TAK-981 alone (Fig. 7J and K, right). Notably, the levels of H3K27ac at ^{PPRE1}*UCP1* were weaker compared to ^{PPRE2}*UCP1*, a pattern consistent with previous ChIP-seq data from beige adipocytes (Suppl. Fig. S2C) (Loft *et al*, 2015) and reflecting our *UCP1* expression data. A similar trend was observed when assessing *PGC1A* and *CIDEA* PPREs, although the effects of TAK-981 and rosiglitazone were slightly less pronounced than for *UCP1*, particularly for H3K27ac at the PPRE of *CIDEA* (Fig. 7J and K, right). Nonetheless, these data are consistent with a model in which transient inhibition of SUMOylation facilitates the epigenetic activation of PPREs at thermogenic enhancers.

Discussion

The cellular mechanisms that control identity conversion from white to beige adipocytes remain poorly understood. In this study we revealed a key role for SUMO in this process. While inhibiting SUMOylation alone was not sufficient to cause beiging, the small-molecule SUMOylation inhibitor TAK-981 synergized with the clinically approved PPARG agonist rosiglitazone to induce conversion of white adipocytes into beige adipocytes. This was evidenced by substantial transcriptional reprogramming, it involved increased expression of the thermogenic protein UCP1 and resulted in strong mitochondrial uncoupling. These results are consistent with a model in which SUMOylation serves as a barrier of transcriptional programs to maintain white cell's identity (Fig. 7L).

WAT plasticity allows adaptive thermogenesis, which may occur via two routes: either through *de novo* differentiation of white/beige precursors into beige cells or the

reversible conversion of white cells into beige cells (Merrick *et al.*, 2019; Roh *et al*, 2018; Schwalie *et al.*, 2018; Shao *et al*, 2019). Whether one of these routes is favored during hypothermia or whether both contribute to beiging remains a topic of debate. In this study, transient SUMOylation inhibition enabled beiging in both adipose stem cells and mature adipocytes in the presence of rosiglitazone. This strongly suggests that beiging transcription programs are imprinted in adipose stem cells and retained in white adipocytes, priming them to respond to hypothermia.

Beiging has been shown to be reversible, i.e. beige cells can revert to white adipocytes upon warming (Roh *et al.*, 2018). However, we found that inhibition of SUMOylation by TAK-981 imprinted a stable beiging fate that was not reversed by washing out the drug even 32 days after treatment. This observation suggests that temporal relief of the SUMO barrier allows cells to assume a new equilibrium that may involve implementation of a stable beige adipocyte epigenetic memory. This is consistent with our recent findings that SUMOylation also preserves and prevents conversion of adipocytes into osteoblasts, further underscoring the role of SUMOylation in regulating adipose tissue identity, plasticity, and function (Bjune *et al*, 2023).

Although the transcriptomes of white and beige adipocytes largely overlap, beiging involves extensive transcriptional remodeling, leading to a functional shift from energy storage to energy expenditure. This process is driven by the activation of beige-specific genes such as *UCP1*, *CIDEA* and *ELOVL3* (Inagaki *et al.*, 2016). Our data show that transient SUMOylation inhibition stably shifts the transcriptome toward beiging in a rosiglitazone-dependent manner.

The ability of transient hypoSUMOylation to induce a stable transcriptional and cellular fate change suggests that SUMOylation plays a key role in epigenetic regulation in hASCs and mature adipocytes, as previously shown in ESCs and beige cells (Bjune *et al.*, 2023; Cossec

et al., 2018). Specifically, transient SUMOylation inhibition leads to derepression of the beiging transcriptional program, implying that SUMOylation actively enforces beiging gene silencing to limit adaptive thermogenesis. In support, our study of thermogenic enhancers suggests that while SUMOylation inhibition primarily affects chromatin accessibility by facilitating histone acetylation at *UCP1* PPREs, the presence of rosiglitazone is necessary to achieve maximal UCP1 expression. This supports a model in which SUMOylation inhibition leads to epigenetic remodeling, whereas rosiglitazone enhances *UCP1* transactivation via PPARG (Suppl. Fig. S2D).

Increased expression of UCP1 upon treatment with rosiglitazone and TAK-981 was reflected in a metabolic shift with higher OCR and ECAR. As reported by others, UCP1-induced OCR was not correlated with increased mitochondrial ATP production, but instead increased thermogenesis (Nyman *et al*, 2017). Our results confirm that UCP1 is not associated with ATP synthesis. Rather, we observed increased glycolysis associated with increased ATP production. This phenotype suggests that differentiated cells display a glycolytic and highly energy demanding phenotype, which has been demonstrated by others (Aydemir *et al*, 2020). Interestingly, cells differentiated in the presence of rosiglitazone and TAK-981were more glycolytic compared to regular brown adipocyte. This suggests that rosiglitazone together with TAK-981 induces a highly energy consuming fat cell phenotype which may contribute to explain their therapeutic use.

How might SUMO work as a cell epigenetic identity barrier in white adipocytes at the molecular level? Prior mass spectrometry and RIME experiments in adipocytes and other cell types have suggested that SUMOylation of chromatin-bound proteins within heterochromatin-maintaining complexes restricts adaptive gene activation and transcriptional reprogramming (Launonen *et al.*, 2024; Paakinaho *et al*, 2021; Theurillat *et al*, 2020; Zhao *et al.*, 2022). Furthermore, our data reveal that transient SUMOylation inhibition in hASCs

leads to a stable reduction in H3K27me3 at beiging enhancers even after SUMOylation recovery, suggesting that TAK-981 disrupts Polycomb-mediated histone methylation, ultimately establishing a stable epigenetic beiging fate. A similar link between PRC2, H3K27me3, SUMOylation, and energy metabolism preservation in adipocytes and cancer cells has been proposed (Chen *et al*, 2018; Zhao *et al*, 2024). These findings mirror a recent study in *Drosophila*, where transient Polycomb downregulation resulted in stable epigenetic reprogramming toward a cancerous state (Parreno *et al*, 2024). This raises the possibility that SUMOylation serves as a key regulator of Polycomb, maintaining H3K27me3 homeostasis to prevent epigenetic drift towards unwanted identity conversion or into disease states (Suppl. Fig S2D). These insights are also relevant to energy storage in obesity, which has been linked to an epigenetic obesogenic memory (Hinte *et al.*, 2024).

In parallel, we observed a stable increase in H3K27ac levels at beiging enhancers depleted of H3K27me3, suggesting that SUMOylation inhibition facilitates histone acetylation, a process known to contribute to *UCP1* expression via HAT1 (Li *et al*, 2016). Consistently, recent studies have identified HATs as major SUMO targets across various cell types, reinforcing the idea that SUMOylation regulates histone acetylation (Hendriks *et al.*, 2018; Launonen *et al.*, 2024; Paakinaho *et al.*, 2021; Theurillat *et al.*, 2020; Zhao *et al.*, 2022). Further investigation using techniques such as RIME (Launonen *et al.*, 2024) is needed to determine whether SUMOylation of chromatin-bound factors enforces an epigenetic and transcriptional memory of beiging in hASCs and throughout adipocyte differentiation (Supll. Fig. S2D). This is the focus of our ongoing studies.

During adaptive thermogenesis, activation of the cAMP-PKA-p38 signaling pathway mobilizes specific transcription factors (TFs) and coactivators to induce the expression of beiging genes. Our data suggest that SUMOylation inhibition activates this pathway at two levels. RNA sequencing revealed that SUMOylation facilitates the repression of genes

involved in this signaling cascade, though the precise mechanism remains unclear. Additionally, western blot analysis of PKA and p38 substrates phosphorylation suggests that SUMOylation may also suppress the activity of these kinases. Since both PKA and p38 have been identified as SUMOylation targets (Wang *et al*, 2021), SUMOylation could directly inhibit their enzymatic activity or modify their substrate specificity. These findings support a model in which SUMOylation acts as a regulatory constraint on cAMP-PKA-p38 signaling, thereby restricting the initiation of beiging (Fig. 7L).

SUMOylation may also directly modulate transcriptional regulators. SUMOylation has been shown to restrict the transactivation activity of nuclear receptors, including PPARs (Bjune *et al.*, 2023; Katafuchi *et al.*, 2018; Paakinaho *et al.*, 2021). Thus, TAK-981 may directly enhance the transcriptional activity of PPARA/PPARG, boosting the expression of key beiging genes like UCP1. Furthermore, recent studies suggest that preventing the SUMOylation of transcriptional activators, including nuclear receptors and coactivators, can alter their chromatin localization (Launonen *et al.*, 2024; Paakinaho *et al.*, 2021; Rosonina *et al.*, 2017; Sri Theivakadadcham *et al*, 2019; Valima *et al*, 2025; Zhao *et al.*, 2022). Our recent findings show that chronic SUMOylation inhibition in differentiating 3T3-L1 cells disrupts the chromatin occupancy of RXR, leading to significant changes in pre-adipogenic and adipogenic gene expression (Zhao *et al.*, 2022). Given that rosiglitazone is a PPARG agonist, its effect on chromatin localization, along with other activators and coactivators, may be influenced by TAK-981. This suggests that TAK-981 could help reprogram the transcriptome toward beiging by stabilizing the recruitment of PPAR-RXR and coactivators at enhancers such as those controlling UCP1.

It is worth mentioning that our findings are in apparent contrast with studies on WAT-specific SENP2 knockout (KO) mice (Lee *et al*, 2022). These mice lack the deSUMOylase SENP2, leading to increased SUMOylation levels of certain proteins, such as C/EBPβ. The

increased SUMOylation of C/EBPβ inhibits its function, resulting in lower expression of HOXC10, a browning inhibitor, through recruitment of the transcriptional repressor DAXX. As a consequence, higher SUMOylation levels in WAT enhanced beiging capacity (Lee *et al.*, 2022). We do not presently understand why we observed the opposite phenotype, where loss of SUMOylation leads to increased beiging. One possible explanation could be differences in the dynamics of the process. In cell lacking SENP2, SUMO levels are chronically increased, which may have a much wider impact on transcriptional programs, including secondary effects and activation of compensatory mechanisms that may not be operative under physiological conditions. It is also possible that SUMO serves as a rheostat, in which either too little SUMOylation or too much SUMOylation lead to the same phenotype, i.e. beiging. Clearly, more work is needed to clarify these differences. Nonetheless, from a therapeutic perspective our approach using TAK-981 offers a distinct advantage. As a small-molecule inhibitor, TAK-981 can be used transiently to induce reprogramming of adipose tissue.

In this study, we characterized the stable transcriptional and cellular identity shifts initiated by transient SUMOylation inhibition, as well as chromatin modifications at selected beiging enhancers several days after TAK-981 treatment. Our findings suggest that TAK-981 imprints a stable beiging fate, priming cells to respond more robustly to rosiglitazone. These findings may provide new inroads in treatment of metabolic disorders using carefully defined sequential drug treatment algorithms.

Materials and Methods

Cell culture, differentiation and treatments

Human white pre-adipocytes (hTERT-A41hWAT-SVF, ATCC, CRL-3386) were maintained and differentiated based on previously established protocols (Herbers *et al*, 2022). Cells were maintained in StableCell^{TM} DMEM High Glucose Medium (Sigma, D0819), supplied with 10% Fetal Bovine Serum (FBS, F7524) and 1% Penicillin/Streptomycin (PenStrep, Gibco, 15140-122) at 37°C in a humidified incubator at 5% CO_2 in air atmosphere.

In advance to differentiation induction, the pre-adipocytes were grown to full confluence and kept at full confluence for 2 days. After two days at full confluency, differentiation was induced by adding StableCell^{TM} DMEM High Glucose Medium, supplied with 2% FBS, 1% PenStrep, 1 µM Dexamethasone (D4902, Sigma), 0.5 mM 3-Isobutyl-1-methylxanthine (I5879, Sigma), 0.1 µM human insulin (91077C, Sigma), 17 µM Pantothenate (P5155, Sigma), 22 µM Biotin (B4639, Sigma) and 1 µM Rosiglitazone (R2408, Sigma) for 7 days. On Day 7 (D7), the induction medium was replaced with the maintenance medium, consisting of StableCell^{TM} DMEM High Glucose Medium, supplied with 2% FBS, 1% PenStrep, 1 µM Dexamethasone, 0.1 µM human insulin, 17 µM Pantothenate and 22 µM Biotin for at least 14 days. The medium was refreshed every second or third day.

Human brown pre-adipocytes (hTERT-A41hBAT-SVF, ATCC, CRL-3385) were differentiated based on previously established protocols (Wang *et al*, 2020). SVF cells were seeded and grown to full confluency as described above. After two days at full confluency, the induction medium was added (StableCell^{TM} DMEM High Glucose Medium, supplied with 2% FBS, 1% PenStrep, 2µg/ml Dexamethasone, 0.5 mM 3-Isobutyl-1-methylxanthine, 5 µg/ml human insulin, 1 µg/ml Rosiglitazone and 50 nM T3. Differentiation was induced for two days, followed by changing to differentiation medium (StableCell^{TM} DMEM High Glucose Medium with 3-Isobutyl-1-methylxanthine, human insulin, Rosiglitazone and T3 as before).

The SUMOylation inhibitor TAK-981 (Takara) was added at 0.5 µM to the cells at the indicated days for 48hrs. After the treatment, the cells were washed with phosphate-buffered saline (PBS) and differentiation continued as indicated.

Lipid staining

Differentiated adipocytes were washed with PBS and fixed in 10% formaldehyde for 45 minutes at room temperature. Cells were permeabilized with 60% isopropanol for 5 minutes at room temperature and stained with Oil Red O (Sigma-Aldrich, MAK194) for 15 minutes at room temperature. After 3 – 5 washes in mqH_2O the staining was assessed under a Brightfield Microscope and a regular camera.

Total RNA extraction

Cells were collected in TRIzole Reagent (Life Technologies, MAN0001271) and 200µL of chloroform was added per 1ml of TRIzole Reagent used. Samples were vortexed thoroughly and incubated on ice for 5 minutes before centrifugation at 13,200 RPM for 10 minutes at 4°C. The aqueous phase containing the RNA was collected and the RNA precipitated with 100% isopropanol and incubated on ice for 5 minutes. The RNA pellets were centrifuged at 13,200 RPM for 10 minutes at 4°C. The supernatant was removed and the RNA pellet washed in 70% ethanol, followed by incubation on ice for 5 minutes. After centrifugating the RNA at 13,200 RPM for 5 minutes at 4°C the supernatant was removed, and the RNA pellet briefly air dried. Finally, the RNA was resuspended in RNAse-free H_2O and incubated on ice for 20 minutes. RNA concentrations were determined using Nanodrop 3000.

Reverse transcription and RT-qPCR

Total RNA was reverse transcribed using the QuantiTect Reverse Transcription Kit according to manufacturer's instructions (Qiagen, 205313).

RT-qPCR was performed using the HOT FIREPol® EvaGreen® qPCR Supermix (Solis Biodyne, 08-36-00001-5) on a LightCycler 96 instrument (Roche Diagnostics). Gene expression was normalized to the expression of *18S* and plots and data analyzed and visualized using GraphPad Prism 9. *P values* are indicated in figure legends. Primer sequences used in this study are listed in Table 1.

Table 1 Oligonucleotides used in this study.

Oligonucleotide	Sequence (5' - 3')	Use
18S_F	GCAGAATCCACGCGCCAGTACAAG	RT-qPCR
18S_R	GCTTGTTGTCCAGACCATTGGC	
CEBPA_F	GACTTGGTGCGTCTAAGATGAG	
CEBPA_R	GGCATTGGAGCGGTGAGTT	
CEBPB_F	AGAAGACCGTGGACAAGCACAG	
CEBPB_R	CTCCAGGACCTTGTGCTGCGT	
PPARG_F	ACTCTGGGAGATTCTCCTATT	
PPARG_R	CTCCATAGTGAAATCCAGAAG	
ADPQ_F	CAGGCCGTGATGGCAGAGATG	
ADPQ_R	GGTTTCACCGATGTCTCCCTTAG	
UCP1_F	ACCGCAGGGAAAGAAACAGC	
UCP1_R	TCAGATTGGGAGTAGTCCCT	
CTRL_F	GCCCTCCTGGGATTAAA	ChIP-qPCR
CTRL_R	CATTCCATTCCCACGAAC	
hUCP1_PPRE1_F	GCTCTCCCAGAAGGAAG	
hUCP1_PPRE1_R	GAGGAAGGAGGATGAGAAG	
hUCP1_PPRE2_F	CTGGCTTCACCACTTCT	
hUCP1_PPRE2_R	GGGATACCACCCTCTCC	
hPGC1A_PPRE1_F	TGACTTGTGTTTCTGTTATGG	
hPGC1A_PPRE1_R	CTACCTCTCCGACATGTTT	
hPGC1A_PPRE2_F	GGCTTCTCAAATATCACAAGAG	
hPGC1A_PPRE2_R	GAGAACATGAAATCAAATTGGC	
hCIDEA_PPRE_F	CAGCCCTGTTCTTTCTATG	
hCIDEA_PPRE_R	CCCAATGTGATGGATGAG	

hTSHR_PPRE1_F	CCAGCCAAGGAAAGTGAA	
hTSHR_PPRE1_R	TCACCACTGTGGAGGAG	
hTSHR_PPRE2_F	TTCTCTGGTGTTCATTTGTAG	
hTSHR_PPRE2_R	AAACCATAGGGACAGGAAA	
hACSL1_PPRE_F	GCAGTGAACCGTGATTG	
hACSL1_PPRE_R	TCAGCTTGACCCAGAAA	

RNA sequencing

Library preparation and sequencing

Total RNA was extracted as described in 'RNA purification'. Samples were cleaned using the RNeasy Mini Kit (Qiagen, 74104) and gDNA removed using the on-column RNase-free DNase set (Qiagen, 79254). RNA quality and concentration were assessed using an Agilent Bioanalyzer device using the RNA 6000 Nano Kit (Agilent, 5067-1511).

Total RNA-Seq libraries were generated from 200 ng of total RNA using Illumina Stranded Total RNA Prep, Ligation with Ribo-Zero Plus kit and IDT for Illumina RNA UD Indexes, Ligation (Illumina, San Diego, USA), according to manufacturer's instructions. DNA libraries were amplified using 15cycles of PCR. Surplus PCR primers were further removed by two successive purifications using SPRIselect beads (Beckman-Coulter, Villepinte, France). The final libraries were checked for quality and quantified using Bioanalyzer 2100 system (Agilent technologies, Les Ulis, France). Sequencing was performed on the GenomEast platform (IGBMC, Illkirch, France) with 1x50 bp on a NextSeq 2000 System (Illumina).

RNA-sequencing analysis

Reads were preprocessed to remove adapter, polyA and low-quality sequences (Phred quality score below 20). After this preprocessing, reads shorter than 40 bases were discarded for further analysis. These preprocessing steps were performed using cutadapt (Martin, 2011)

version 4.2. Reads were mapped to rRNA sequences of RefSeq and GenBank databases using bowtie (Langmead & Salzberg, 2012) version 2.2.8. Reads mapping to rRNA sequences were removed for further analysis. Reads were mapped onto the GRCh38 assembly2 of Homo sapiens genome using STAR (Dobin *et al*, 2013) version 2.7.10b. Gene expression quantification was performed from uniquely aligned reads using htseq-count (Martin, 2011) version 0.13.5, with annotations from Ensembl version 110 and "union" mode3. Only non-ambiguously assigned reads to a gene have been retained for further analyses.

Differential gene expression analyses

RNA-seq raw count data per ENSEMBL ID were analyzed using *DESeq2* (v1.44.0) (Love *et al*, 2014) within the *R* (v4.4.2) programming environment to perform differential gene expression analyses between conditions. A gene was considered differentially expressed with a log2 fold-change (log2FC) cutoff of ±1 and an adjusted p-value (padj) < 0.05 (Benjamini-Hochberg method).

Functional enrichment analyses

The *biomaRt* package (v2.60.1) (Durinck *et al*, 2009) was used to map ENSEMBL IDs to gene symbols. Gene Ontology (GO) enrichment analysis for GO biological processed (GO BP) was performed using the *clusterProfiler* package (v4.12.6) (Yu *et al*, 2012) with differentially expressed genes (up- or down-regulated) as input. The enrichment results were visualized using dotplots for the ratio of genes considered in the 10 most enriched GO BP terms, where the size of each dot represents the number of up-regulated genes in a GO BP, and color indicates the adjusted p-value (see Fig. 5B) when considering genes up-regulated (resp. down-regulated) in TAK-981 + Roziglitazone versus Roziglitazone).

Volcano plot visualization

Volcano plots were generated using *EnhancedVolcano* (v1.22.0) (Blighe, 2018) for visualizing differential expression analyses, highlighting genes of interest with log2FC > 1 or < -1 and/or padj < 0.05 (Fig. 4A-C and Fig. 5A). When considering the differential expression results between conditions TAK-981 + Rosiglitazone vs Rosiglitazone, (Fig. 5A), beiging-related genes (i.e., associated with GO BP "temperature homeostasis," "positive regulation of cold-induced thermogenesis," and "brown fat cell differentiation") were labeled explicitly in the plot.

Heatmap visualization

Expression of differentially expressed (DE) genes upregulated in TAK-981 + Rosiglitazone versus Rosiglitazone and associated with beiging (see above) was visualized as a heatmap using *ComplexHeatmap* (v2.20.0) (Gu *et al*, 2016) (Fig. 5C). Gene expression values were z-score normalized across conditions. Experimental groups (with replicates) are provided as columns. DE genes are provided as rows. Fig. 4D-F provides similar heatmap representations of differentially expressed genes when comparing different conditions (last 6 rows) and considering genes (columns) associated with the top 10 most enriched GO BP terms (first 10 rows).

Transcription factor activity analysis

TF activity inference was performed using the *decoupler* (v1.8.0) package in Python (v3.11.7) (Badia *et al.*, 2022). Log2 fold-change values of upregulated DE genes were used to infer TF activities with the Universal Linear Model method. TF-target interaction networks were obtained from OmniPath (Turei *et al.*, 2021).

Fig. 7B presents bar plots depicting the inferred most active TFs when comparing TAK-981 + Rosiglitazone versus Rosiglitazone. Fig. 7C-D and Supplementary Fig. 2B show volcano plots of the log2FC and adjusted p-values of the expression of beiging targets of PPARA, PPARG, and SREBP1, respectively.

Thermogenesis pathway visualization

The "Thermogenesis" KEGG pathway was visualized with differentially expressed genes between TAK-981 + Rosiglitazone versus Rosiglitazone using the *pathview* (v1.44.0) R package (Luo & Brouwer, 2013) (Supplementary Fig. 3A).

Protein extraction and western blotting

For UCP1 detection and PKA phosphor-substrates detection by Western Blot, cells were washed in ice-cold PBS prior lysis in ice-cold RIPA buffer (50mM Tris-HCl pH 7.5, 150mM NaCl, 5mM EDTA, 1% NP-40, 0.5% Sodium deoxycholate, 0.1% SDS), freshly supplied with protease inhibitor (Roche). Lysates were centrifuged at 13,000 rpm for 10 minutes at 4°C. To eliminate lipid carryover, the supernatant was filtered through a RNeasy column (Qiagen, 74104) and centrifuged at 10,000 rpm for 1 min at 4°C. The flow through was collected and protein concentrations were measured with the Braford Assay. 20 - 40µg of protein were used for SDS-PAGE and proteins of interest detected by Western Blots.

For SUMO2/3, p38, p-p38, p-ATF2, p-ATF1 and p-CREB Western Blots, cells were lysed in 2x Laemmli Buffer and sonicated for 2 cycles (30 sec on/30 sec off). Lysates were centrifuged at 13,000 rpm for 10 minutes at 4°C. To eliminate lipid carryover, the supernatant was filtered through a RNeasy column (Qiagen, 74104) and centrifuged at 10,000 rpm for 1 min at 4°C. Protein concentrations were determined with the Bradford Assay. 15 – 50µg of protein were used for SDS-PAGE and proteins of interested detected by Western Blots.

The following antibodies were used: UCP1, abcam, ab209483; PKA phosphor-substrates, Cell Signaling 9624; p-CREB / p-ATF1, Cell Signaling 9198; p38 MAPK, Cell Signaling 9212; p-p38 MAPK, Cell Signaling 9211; p-ATF2, Cell Signaling 24329; SUMO2/3, abcam, ab81371 and TBP, Protein Tech, 22006-1-AP). Quantifications were performed using FiJi (Schindelin *et al*, 2012).

Mitochondrial respiration analysis

Human white adipocytes were differentiated as described in 'Cell culture, differentiation and treatment' in 24 multiwell plates (Seahorse). OCR and ECAR were measured using the XF Cell Mito Stress Test on a XF24 extracellular Flux Analyzer (Seahorse Agilent). During the assay, 2µM Oligomycin (O4876, Sigma) and 2.5µM BAM15 (HY-110284, MedChemExpress) were added as indicated.

Chromatin immunoprecipitation (ChIP)

Human white adipocytes were differentiated as described in 'Cell culture, differentiation and treatment' in 10cm-dishes. Cells were washed twice in PBS and collected in Digitonin lysis buffer with sodium-butyrate (10mM Tris-HCl, pH 7.4, 10mM NaCl, 3mM $MgCl_2$, 20mM Sodium-butyrate, 0,01% Digitonin, 0.1% Tween-20, 0.1% NP-40) (Corces *et al*, 2017). To obtain nuclei, the cells were dounced (35 strokes) using pestle B. Cell lysis was assessed and confirmed with a phase-contrast microscope. Nuclei were centrifuged at 500g for 10 min at 4°C. The nuclei pellet was washed twice in Digitonin lysis buffer and resuspended in nuclear pellet buffer NPB (10mM HEPES, 1.5 $MgCl_2$, 250mM sucrose, 0.1% NP-40, protease inhibitor cocktail, 1mM PMSF and 20mM Sodium-butyrate in PBS). Chromatin was crosslinked with 1% Formaldehyde for 8 min. Formaldehyde was neutralized using 125mM Glycine for 10min. After two washes with NPB, the nuclei were resuspended

in nuclear lysis buffer (50 mM Tris-HCl pH 7.5, 1% SDS, 10 mM EDTA, 20 mM N-ethyl maleimide and protease inhibitor cocktail) and incubated at 4°C for 2 h. Lysates were sonicated for 10 cycles (30 s on/30 s off) at 4°C using a Bioruptor Pico sonicator (Diagenode). After sonication, lysates were centrifuged at 14,000 rpm for 10 min at 4°C. Protein concentration was assessed using the Bradford assay and 30 µg protein used for histone immunoprecipitation. Input samples (10 µg) were saved. Samples were diluted 10-fold in the immunoprecipitation buffer (1.1% Triton X100, 50 mM Tris-HCl, pH 7.5, 167 mM NaCl, 5 mM N-ethyl maleimide, 1 mM EDTA, 0.01% SDS and protease inhibitor cocktail). Immunoprecipitations were carried out with antibodies for H3K27ac (ab4729, abcam), H3K27me3 (C15410195, Diagenode), H3K9me3 (ab8898, abcam) and Dynabeads Protein A or G (10002D, 10004D, ThermoFisher Scientific) overnight at 4°C. Beads were then washed 2 times in low-salt buffer (50 mM Tris-HCl, pH 7.5, 150 mM NaCl, 1% Triton X100, 0.1% SDS, 1 mM EDTA), 2 times in high-salt buffer (50 mM Tris-HCl, pH 7.5, 500 mM NaCl, 1% Triton X100, 0.1% SDS, 1 mM EDTA) and in TE buffer (10 mM Tris-HCl, pH 7.5, 0.2% Tween-20, 1 mM EDTA). Elution was done two time in 50µl of 100 mM NaHCO3, 1%SDS at 65◦C for 10 min under agitation. Chromatin crosslinking was reversed at 65°C for 5 h with 280 mM NaCl and 0.2 µg/ml RNase DNase free (11119915001, Roche). Proteins were then digested using 0.2 µg/ml of Proteinase K (03115828001, Roche) during 1 h at 65°C. DNA from immunoprecipitations and inputs were purified using the Qiagen PCR purification kit. The resulting samples were further used for qPCR as described before.

Genome tracks

The UCSC genome browser (Kent *et al*, 2002) (hg19) was used to generate Fig. S2C. The GENCODE V47lift37 (Frankish *et al*, 2023), NCBI RefSeq (Pruitt *et al*, 2014), and HGNC (Tweedie *et al*, 2021) tracks provide information about gene annotations. The

JASPAR CORE 2024 track (Rauluseviciute *et al.*, 2024) was filtered to provide transcription factor binding site (TFBS) predicted with JASPAR profiles associated with Ppara (MA2338.1), PPARA::RXRA (MA1148.2), PPARG (MA0066.2), and Pparg::Rxra (MA0065.3). The PPRE_hg19.bed track provides the localization of the TFBSs considered to design the amplicons, which were lifted over from hg38 to hg19. The tracks PPARGbriteRep1 and PPARGbriteRep2 represents bigWig of two PPARG ChIP-seq replicate experiments in mature human adipose-derived stem cells (Loft *et al.*, 2015) and were obtained from GEO (GSM1443810 and GSM1443812). The tracks H3K27acBriteRep1 and H3K27acBriteRep2 represents bigWig of two H3K27ac ChIP-seq replicate experiments from the same cell types (Loft *et al.*, 2015) and were obtained from GEO (GSM1443806 and GSM1443808).

Funding

PC was supported by the Research Council of Norway (Grant numbers 301268 and 353961), by institutional support from the University of Oslo and by UNIFOR. Sequencing was performed by the GenomEast platform, a member of the 'France Génomique' consortium (ANR-10-INBS-0009). AM is supported by funding from the Research Council of Norway (187615), Helse Sør-Øst, and the University of Oslo through the Centre for Molecular Medicine Norway (NCMM) and from the Norwegian Cancer Society (215027, 272930). BSS is supported by the Throne Holst Foundation Grant 2023 to 2025. JME was supported by grants from the Norwegian Health Authority South-East, grant numbers 2019049, 2019096 and 2025077; the Norwegian Cancer Society, grant 208012; and the Research Council of Norway through its Centers of Excellence funding scheme (262652) and through grant 314811.

Acknowledgements

We thank Prof. Simon N. Dankel, Prof. Gunnar Mellgren, Dr. Jan-Inge Bjune and Dr. Damien Dufour for their input.

Data availability

RNA sequencing data is available at the Gene Expression Omnibus using accession number GSE290926. H3K27ac and PPARG ChIP-seq datasets were downloaded from the GEO using accession number GSM1443810, GSM1443812, GSM1443806 and GSM1443808.

Author contributions

Patrizia Maria Christiane Nothnagel: Investigation, Formal analysis, Visualization, Writing - Original Draft. **Jonas Aakre Wik:** Methodology, Investigation. **Nolwenn Briand:** Supervision, Methodology, Investigation. **Yunna E. Strøm:** Investigation. **Magnar Bjørås:** Funding acquisition, Resources. **Jorrit M. Enserink:** Resources, Writing - Review & Editing. **Bjørn Steen Skålhegg:** Supervision, Methodology, Writing - Review & Editing. **Anthony Mathelier:** Methodology, Investigation, Formal analysis, Visualization, Funding acquisition, Writing - Review & Editing. **Pierre Chymkowitch:** Conceptualization, Methodology, Resources, Supervision, Funding acquisition, Writing - Original Draft, Writing - Review & Editing.

Fig. legends

Fig. 1: Analysis of transient sumoylation inhibition in hASCs and its impact on adipogenic and beiging markers.

(A) Schematic representation of the experimental setup.

(B) Validation of transient SUMOylation inhibition by SUMO2/3 western blot at the indicated time points.

(C) Time-course analysis of *PPARG* mRNA expression under the conditions described in *(A)*. Data represent the mean ± standard deviation (SD) from at least three independent experiments.

(D) Time-course analysis of *UCP1* mRNA expression under the conditions described in *(A)*. Data represent the mean ± SD from at least three independent experiments.

(E) Western blot analysis of UCP1 protein levels at indicated time points. Brown cells lysate (BAT) was used as a positive control.

Fig. 2: Analysis of transient sumoylation inhibition in mature adipocytes and its impact on adipogenic and beiging markers.

(A) Schematic representation of the experimental setup.

(B) Validation of transient SUMOylation inhibition by SUMO2/3 western blot at the indicated time points.

(C-D) Time-course analysis of *PPARG* mRNA expression from day 0 to day 21 post-adipogenic induction *(C)* and from day 22 to day 32 post-adipogenic induction *(D)*. Data represent the mean ± standard deviation (SD) from at least three independent experiments. Statistical significance was calculated using two-way ANOVA in GraphPad Prism 10 (adjusted p-value: $p < 0.05$, $p < 0.005$, $p < 0.0005$, $p < 0.0001$).

(E-F) Time-course analysis of *UCP1* mRNA expression from day 0 to day 21 post-adipogenic induction *(E)* and from day 22 to day 32 post-adipogenic induction *(F)*. Data represent the mean ± SD from at least three independent experiments. Statistical significance

was calculated using two-way ANOVA in GraphPad Prism 10 (adjusted p-value: $p < 0.05$, $p < 0.005$, $p < 0.0005$, $p < 0.0001$).

(G) Western blot analysis of UCP1 protein levels at day 22 and day 32 post-adipogenic induction. Brown cells lysate (BAT) was used as a positive control.

(H) Summary of findings from Fig. 1 and 2, suggesting that transient SUMOylation inhibition promotes both the de novo differentiation of beige adipocytes from hASCs and the transdifferentiation of white adipocytes into beige adipocytes.

Fig. 3: Metabolic asessment of TAK-981 and rosiglitazone effects on mitochondrial uncoupling.

(A) Schematic representation of the experimental setup for the measurement of oxygen consumption rate (OCR) and extracellular acidification rate (ECAR) after transient SUMOylation inhibition in hASCs.

(B-D) Measurement of oxygen consumption rate (OCR) *(B)*, extracellular acidification rate (ECAR) *(C)*, and integrated OCR/ECAR analysis *(D)* to assess the effect of TAK-981 and rosiglitazone on mitochondrial uncoupling and energy expenditure in hASCs, 22 days post-adipogenic induction.

(E) Schematic representation of the experimental setup for the measurement of OCR and ECAR after transient SUMOylation inhibition in adipocytes.

(F-H) Measurement of OCR *(F)*, ECAR *(G)*, and integrated OCR/ECAR analysis *(H)* to assess the effect of TAK-981 and rosiglitazone on mitochondrial uncoupling and energy expenditure in mature adipocytes, 32 days post-adipogenic induction.

Fig. 4: Differential gene expression and gene ontology analysis of hASCs and adipocytes following Rosiglitazone and TAK-981 treatments compared to untreated cells.

(A) Volcano plot showing Differentially Expressed Genes (DEGs) resulting from the treatment of hASCs with rosiglitazone. DEGs were identified by comparing rosiglitazone-treated cells to untreated (CTRL) cells.

(B) Volcano plot showing DEGs resulting from the transient treatment of hASCs with TAK-981. DEGs were identified by comparing TAK-981-treated cells to untreated (CTRL) cells.

(C) Volcano plot showing DEGs resulting from the priming of hASCs with transient SUMOylation inhibition (TAK-981) followed by treatment with rosiglitazone. DEGs were identified by comparing TAK-981 + Rosiglitazone-treated cells to untreated (CTRL) cells.

(D) Gene Ontology (GO) analysis of Biological Processes associated with the DEGs identified in *(A)*.

(E) Gene Ontology (GO) analysis of Biological Processes associated with the DEGs identified in *(C)*.

(F) Gene Ontology (GO) analysis of Biological Processes associated with the DEGs identified in *(E)*.

Fig. 5: Transcriptomic analysis of hASCs primed by transient SUMOylation inhibition and treated with Rosiglitazone.

(A) Volcano plot displaying differentially expressed genes (DEGs) in hASCs primed by transient SUMOylation inhibition (TAK-981) and treated with rosiglitazone, compared to hASCs treated with rosiglitazone alone.

(B) Gene Ontology (GO) analysis (Biological Processes) of upregulated genes identified in *(A)*, highlighting enrichment in pathways associated with adaptive thermogenesis and brown adipocyte differentiation.

(C) Heatmap illustrating the upregulation of key beiging-associated genes in hASCs primed by TAK-981 and treated with rosiglitazone, compared to treatment with rosiglitazone alone.

(D) Gene Ontology (GO) analysis (Biological Processes) of downregulated genes identified in *(A)*.

Fig. 6: Investigating the role of SUMOylation in cAMP-PKA-p38 signaling and adaptive thermogenesis.

(A) Hypothesis: SUMOylation inhibits the cAMP-PKA-p38 signaling pathway, limiting adaptive thermogenesis.

(B) Heatmap showing the stable upregulation of most genes involved in adaptive thermogenesis and cAMP-PKA-p38 signaling in hASCs treated with transient SUMOylation inhibition and rosiglitazone, 22 days after adipogenic induction.

(C) Western blot analysis of PKA substrates phosphorylation, assessed using a pan-PKA-target antibody. TBP was used as a loading control. The asterisk (*) indicates substrates significantly affected by TAK-981 and/or rosiglitazone treatment.

(D) Quantification of PKA substrate signals from *(C)*. The signal for PKA substrates and TBP was quantified using Fiji software, with PKA substrate signals normalized to TBP. Error bars represent the standard deviation of four independent experiments. Student's T-test was used to calculate P-values.

(E) Western blot analysis of the phosphorylation of CREB, ATF1, p38, and ATF2. TBP was used as a loading control.

(F-G-H) Quantification of the signals from *(E)*: p-CREB *(F)*, p-p38 (G) and p-ATF2 *(H)*.

Signals were normalized to TBP for p-CREB and p-ATF2, and to p-p38 for p-p38. Error bars represent the standard deviation of three independent experiments. Student's T-test was used to calculate P-values.

Fig. 7: Transient sumoylation inhibition enhances PPARA/G transactivation and epigenetic changes at beiging enhancers

(A) Hypothesis: SUMOylation restricts the transactivation activity of PPARA/G either directly or indirectly through the cAMP-PKA-p38 axis.

(B) In silico prediction based on RNA-seq data, showing the transcription factors mobilized upon treatment with TAK-981 and rosiglitazone.

(C-D) Volcano plots showing the PPARA-target genes *(C)* and PPARG-target genes *(D)* activated in response to SUMOylation inhibition and rosiglitazone. Differentially expressed genes were identified by comparing TAK-981 + Rosiglitazone-treated cells to Rosiglitazone-treated cells, as described in Fig. 5A and the methodes.

(E-I) Schematics of ChIP-qPCR regions and primer pairs used in the experiments depicted in J and K.

(J-K) ChIP-qPCR assessment of H3K27ac *(J)* and H3K27me3 *(K)* occurrences at beiging enhancers, as illustrated in (E-I). Error bars represent the average to the mean of two independent experiments. ChIP signals were normalized to inputs, and a gene desert at chromosome 12 (CTRL) was used as a negative control. Statistical significance was calculated using a one-sided, homoscedastic Student's t-test, with *$p < 0.05$, **$p < 0.01$, ***$p < 0.001$, and ****$p < 0.0001$.

Supplementary figure legends

Fig. S1: Assessment of adipogenesis and fat accumulation in hASCs and adipocytes upon TAK-981 and Rosiglitazone treatments

(A) Oil-Red-O staining assessment of fat accumulation in hASCs 22 and 32 days after adipogenic induction upon TAK-981 and rosiglitazone treatments.

(B) RT-qPCR analysis of adipogenic marker expression in hASCs 22 and 32 days post adipogenic induction following TAK-981 and rosiglitazone treatments (refer to Fig. 1A). Error bars represent the standard deviation of three independent experiments. Statistical significance was determined using Student's t-test and calculated in GraphPad Prism10 using the 2-way ANOVA test (Adjusted p-values: * $p < 0.05$, ** $p < 0.005$, *** $p < 0.0005$, **** $p < 0.0001$).

(C) Oil-Red-O staining to assess fat accumulation in adipocytes 22, 27, and 32 days after adipogenic induction with TAK-981 and rosiglitazone treatments.

(D) RT-qPCR analysis of adipogenic marker expression in adipocytes 22 and 32 days post adipogenic induction upon TAK-981 and rosiglitazone treatments (refer to Fig. 2A). Error bars represent the standard deviation of three independent experiments. Statistical significance was determined using Student's t-test and calculated in GraphPad Prism10 using the 2-way ANOVA test (Adjusted p-values: * $p < 0.05$, ** $p < 0.005$, *** $p < 0.0005$, **** $p < 0.0001$).

Fig. S2 Visualization of differential gene expression and mechanistic insights into the role of SUMOylation in adipocyte identity conversion

(A) The "Thermogenesis" KEGG pathway was visualized using differentially expressed genes between TAK-981 + Rosiglitazone and Rosiglitazone-treated cells. Pathway visualization was performed using the pathview (v1.44.0) R package.

(B) Volcano plot showing SREBP1-target genes activated in response to transient SUMOylation inhibition and rosiglitazone. DEGs were identified by comparing TAK-981 + Rosiglitazone-treated cells to Rosiglitazone-treated cells (as in Fig. 5A).

(C) Genome track generated using the UCSC genome browser showing the presence of PPARG and H3K27ac at *UCP1* enhancers (studied in Fig. 7G, J, and K).

(D) Model illustrating the effects of transient SUMOylation inhibition and rosiglitazone treatment on heterochromatin factors, HATs, chromatin structure, and PPARG transactivation during the identity conversion of white to beige adipocytes.

References

Antonio Urrutia G, Ramachandran H, Cauchy P, Boo K, Ramamoorthy S, Boller S, Dogan E, Clapes T, Trompouki E, Torres-Padilla M-E *et al* (2021) ZFP451-mediated SUMOylation of SATB2 drives embryonic stem cell differentiation. *Genes & Development* 35: 1142-1160

Aydemir D, Sarayloo E, Nuray UN (2020) Rosiglitazone-induced changes in the oxidative stress metabolism and fatty acid composition in relation with trace element status in the primary adipocytes. *J Med Biochem* 39: 267-275

Badia IMP, Velez Santiago J, Braunger J, Geiss C, Dimitrov D, Muller-Dott S, Taus P, Dugourd A, Holland CH, Ramirez Flores RO *et al* (2022) decoupleR: ensemble of computational methods to infer biological activities from omics data. *Bioinform Adv* 2: vbac016

Baig MS, Dou Y, Bergey BG, Bahar R, Burgener JM, Moallem M, McNeil JB, Akhter A, Burke GL, Sri Theivakadadcham VS *et al* (2021) Dynamic sumoylation of promoter-bound general transcription factors facilitates transcription by RNA polymerase II. *PLoS Genet* 17: e1009828

Bjune J-I, Laber S, Lawrence-Archer L, Zhao X, Yamada S, Al-Sharabi N, Mustafa K, Njølstad PR, Claussnitzer M, Cox RD *et al* (2023) Mechanisms of the FTO locus association with obesity: Irx3 controls a sumoylation-dependent switch between adipogenesis and osteogenesis. *bioRxiv*: 2023.2010.2017.562662

Blighe KR, S.; Lewis, M. (2018) EnhancedVolcano: Publication-ready volcano plots with enhanced colouring and labeling. *githubcom*

Boulanger M, Chakraborty M, Tempe D, Piechaczyk M, Bossis G (2021) SUMO and Transcriptional Regulation: The Lessons of Large-Scale Proteomic, Modifomic and Genomic Studies. *Molecules* 26

Cao W, Daniel KW, Robidoux J, Puigserver P, Medvedev AV, Bai X, Floering LM, Spiegelman BM, Collins S (2004) p38 mitogen-activated protein kinase is the central regulator of cyclic AMP-dependent transcription of the brown fat uncoupling protein 1 gene. *Mol Cell Biol* 24: 3057-3067

Chang SH, Song NJ, Choi JH, Yun UJ, Park KW (2019) Mechanisms underlying UCP1 dependent and independent adipocyte thermogenesis. *Obes Rev* 20: 241-251

Chen Q, Huang L, Pan D, Zhu LJ, Wang Y-X (2018) Cbx4 Sumoylates Prdm16 to Regulate Adipose Tissue Thermogenesis. *Cell reports* 22: 2860-2872

Christy RJ, Kaestner KH, Geiman DE, Lane MD (1991) CCAAT/enhancer binding protein gene promoter: binding of nuclear factors during differentiation of 3T3-L1 preadipocytes. *Proc Natl Acad Sci U S A* 88: 2593-2597

Chung SS, Ahn BY, Kim M, Choi HH, Park HS, Kang S, Park SG, Kim YB, Cho YM, Lee HK *et al* (2010) Control of adipogenesis by the SUMO-specific protease SENP2. *Mol Cell Biol* 30: 2135-2146

Chymkowitch P, Nguea AP, Aanes H, Koehler CJ, Thiede B, Lorenz S, Meza-Zepeda LA, Klungland A, Enserink JM (2015a) Sumoylation of Rap1 mediates the recruitment of TFIID to promote transcription of ribosomal protein genes. *Genome Res* 25: 897-906

Chymkowitch P, Nguea PA, Aanes H, Robertson J, Klungland A, Enserink JM (2017) TORC1-dependent sumoylation of Rpc82 promotes RNA polymerase III assembly and activity. *Proc Natl Acad Sci U S A* 114: 1039-1044

Chymkowitch P, Nguea PA, Enserink JM (2015b) SUMO-regulated transcription: challenging the dogma. *Bioessays* 37: 1095-1105

Cignarelli A, Melchiorre M, Peschechera A, Conserva A, Renna LA, Miccoli S, Natalicchio A, Perrini S, Laviola L, Giorgino F (2010) Role of UBC9 in the regulation of the adipogenic program in 3T3-L1 adipocytes. *Endocrinology* 151: 5255-5266
Clarke SL, Robinson CE, Gimble JM (1997) CAAT/enhancer binding proteins directly modulate transcription from the peroxisome proliferator-activated receptor gamma 2 promoter. *Biochem Biophys Res Commun* 240: 99-103
Corces MR, Trevino AE, Hamilton EG, Greenside PG, Sinnott-Armstrong NA, Vesuna S, Satpathy AT, Rubin AJ, Montine KS, Wu B *et al* (2017) An improved ATAC-seq protocol reduces background and enables interrogation of frozen tissues. *Nature methods* 14: 959-962
Cossec JC, Theurillat I, Chica C, Bua Aguin S, Gaume X, Andrieux A, Iturbide A, Jouvion G, Li H, Bossis G *et al* (2018) SUMO Safeguards Somatic and Pluripotent Cell Identities by Enforcing Distinct Chromatin States. *Cell Stem Cell* 23: 742-757 e748
Cossec JC, Traboulsi T, Sart S, Loe-Mie Y, Guthmann M, Hendriks IA, Theurillat I, Nielsen ML, Torres-Padilla ME, Baroud CN *et al* (2023) Transient suppression of SUMOylation in embryonic stem cells generates embryo-like structures. *Cell reports* 42: 112380
Cox AR, Chernis N, Kim KH, Masschelin PM, Saha PK, Briley SM, Sharp R, Li X, Felix JB, Sun Z *et al* (2021) Ube2i deletion in adipocytes causes lipoatrophy in mice. *Mol Metab* 48: 101221
Demarque MD, Nacerddine K, Neyret-Kahn H, Andrieux A, Danenberg E, Jouvion G, Bomme P, Hamard G, Romagnolo B, Terris B *et al* (2011) Sumoylation by Ubc9 regulates the stem cell compartment and structure and function of the intestinal epithelium in mice. *Gastroenterology* 140: 286-296
Dobin A, Davis CA, Schlesinger F, Drenkow J, Zaleski C, Jha S, Batut P, Chaisson M, Gingeras TR (2013) STAR: ultrafast universal RNA-seq aligner. *Bioinformatics* 29: 15-21
Dudek AZ, Juric D, Dowlati A, Seymour EK, Ahnert JR, Wang BX, Huszar D, Berger AJ, Friedlander S, Gomez-Pinillos A *et al* (2021) Phase 1/2 study of the novel SUMOylation inhibitor TAK-981 in adult patients (pts) with advanced or metastatic solid tumors or relapsed/refractory (RR) hematologic malignancies. *Journal of Clinical Oncology* 39
Dufour D, Dumontet T, Sahut-Barnola I, Carusi A, Onzon M, Pussard E, Wilmouth JJ, Olabe J, Lucas C, Levasseur A *et al* (2022) Loss of SUMO-specific protease 2 causes isolated glucocorticoid deficiency by blocking adrenal cortex zonal transdifferentiation in mice. *Nat Commun* 13: 7858
Durinck S, Bullard J, Spellman PT, Dudoit S (2009) GenomeGraphs: integrated genomic data visualization with R. *BMC Bioinformatics* 10: 2
Ellis JM, Li LO, Wu P-C, Koves TR, Ilkayeva O, Stevens RD, Watkins SM, Muoio DM, Coleman RA (2010) Adipose Acyl-CoA Synthetase-1 Directs Fatty Acids toward β-Oxidation and Is Required for Cold Thermogenesis. *Cell Metabolism* 12: 53-64
Farmer SR (2006) Transcriptional control of adipocyte formation. *Cell Metab* 4: 263-273
Frankish A, Carbonell-Sala S, Diekhans M, Jungreis I, Loveland JE, Mudge JM, Sisu C, Wright JC, Arnan C, Barnes I *et al* (2023) GENCODE: reference annotation for the human and mouse genomes in 2023. *Nucleic Acids Res* 51: D942-D949
Gu Z, Eils R, Schlesner M (2016) Complex heatmaps reveal patterns and correlations in multidimensional genomic data. *Bioinformatics* 32: 2847-2849
Guilherme A, Yenilmez B, Bedard AH, Henriques F, Liu D, Lee A, Goldstein L, Kelly M, Nicoloro SM, Chen M *et al* (2020a) Control of Adipocyte Thermogenesis and Lipogenesis through β3-Adrenergic and Thyroid Hormone Signal Integration. *Cell reports* 31

Guilherme A, Yenilmez B, Bedard AH, Henriques F, Liu D, Lee A, Goldstein L, Kelly M, Nicoloro SM, Chen M *et al* (2020b) Control of Adipocyte Thermogenesis and Lipogenesis through β3-Adrenergic and Thyroid Hormone Signal Integration. *Cell reports* 31: 107598
Hanssen MJ, Hoeks J, Brans B, van der Lans AA, Schaart G, van den Driessche JJ, Jorgensen JA, Boekschoten MV, Hesselink MK, Havekes B *et al* (2015) Short-term cold acclimation improves insulin sensitivity in patients with type 2 diabetes mellitus. *Nat Med* 21: 863-865
Hendriks IA, Lyon D, Su D, Skotte NH, Daniel JA, Jensen LJ, Nielsen ML (2018) Site-specific characterization of endogenous SUMOylation across species and organs. *Nat Commun* 9: 2456
Herbers E, Patrikoski M, Wagner A, Jokinen R, Hassinen A, Heinonen S, Miettinen S, Peltoniemi H, Pirinen E, Pietilainen KH (2022) Preventing White Adipocyte Browning during Differentiation In Vitro: The Effect of Differentiation Protocols on Metabolic and Mitochondrial Phenotypes. *Stem Cells Int* 2022: 3308194
Hinte LC, Castellano-Castillo D, Ghosh A, Melrose K, Gasser E, Noe F, Massier L, Dong H, Sun W, Hoffmann A *et al* (2024) Adipose tissue retains an epigenetic memory of obesity after weight loss. *Nature*
Inagaki T, Sakai J, Kajimura S (2016) Transcriptional and epigenetic control of brown and beige adipose cell fate and function. *Nat Rev Mol Cell Biol* 17: 480-495
Kalligeros M, Shehadeh F, Mylona EK, Benitez G, Beckwith CG, Chan PA, Mylonakis E (2020) Association of Obesity with Disease Severity among Patients with COVID-19. *Obesity (Silver Spring)*
Katafuchi T, Holland WL, Kollipara RK, Kittler R, Mangelsdorf DJ, Kliewer SA (2018) PPARgamma-K107 SUMOylation regulates insulin sensitivity but not adiposity in mice. *Proc Natl Acad Sci U S A* 115: 12102-12111
Kent WJ, Sugnet CW, Furey TS, Roskin KM, Pringle TH, Zahler AM, Haussler D (2002) The human genome browser at UCSC. *Genome Res* 12: 996-1006
Langmead B, Salzberg SL (2012) Fast gapped-read alignment with Bowtie 2. *Nature methods* 9: 357-359
Langston SP, Grossman S, England D, Afroze R, Bence N, Bowman D, Bump N, Chau R, Chuang B-C, Claiborne C *et al* (2021) Discovery of TAK-981, a First-in-Class Inhibitor of SUMO-Activating Enzyme for the Treatment of Cancer. *Journal of Medicinal Chemistry* 64: 2501-2520
Launonen K-M, Varis V, Aaltonen N, Niskanen EA, Varjosalo M, Paakinaho V, Palvimo JJ (2024) Central role of SUMOylation in the regulation of chromatin interactions and transcriptional outputs of the androgen receptor in prostate cancer cells. *Nucleic Acids Research*
Lee CH, Olson P, Evans RM (2003) Minireview: lipid metabolism, metabolic diseases, and peroxisome proliferator-activated receptors. *Endocrinology* 144: 2201-2207
Lee JS, Chae S, Nan J, Koo YD, Lee SA, Park YJ, Hwang D, Han W, Lee DS, Kim YB *et al* (2022) SENP2 suppresses browning of white adipose tissues by de-conjugating SUMO from C/EBPbeta. *Cell reports* 38: 110408
Li F, Wu R, Cui X, Zha L, Yu L, Shi H, Xue B (2016) Histone Deacetylase 1 (HDAC1) Negatively Regulates Thermogenic Program in Brown Adipocytes via Coordinated Regulation of Histone H3 Lysine 27 (H3K27) Deacetylation and Methylation*. *Journal of Biological Chemistry* 291: 4523-4536

Liu B, Wang T, Mei W, Li D, Cai R, Zuo Y, Cheng J (2014) Small ubiquitin-like modifier (SUMO) protein-specific protease 1 de-SUMOylates Sharp-1 protein and controls adipocyte differentiation. *J Biol Chem* 289: 22358-22364
Liu XZ, Pedersen L, Halberg N (2021) Cellular mechanisms linking cancers to obesity. *Cell Stress* 5: 55-72
Loft A, Forss I, Siersbæk MS, Schmidt SF, Larsen AS, Madsen JG, Pisani DF, Nielsen R, Aagaard MM, Mathison A *et al* (2015) Browning of human adipocytes requires KLF11 and reprogramming of PPARγ superenhancers. *Genes Dev* 29: 7-22
Love MI, Huber W, Anders S (2014) Moderated estimation of fold change and dispersion for RNA-seq data with DESeq2. *Genome biology* 15: 550
Luo W, Brouwer C (2013) Pathview: an R/Bioconductor package for pathway-based data integration and visualization. *Bioinformatics* 29: 1830-1831
Martin M (2011) Cutadapt removes adapter sequences from high-throughput sequencing reads. *2011* 17: 3
Merrick D, Sakers A, Irgebay Z, Okada C, Calvert C, Morley MP, Percec I, Seale P (2019) Identification of a mesenchymal progenitor cell hierarchy in adipose tissue. *Science* 364
Mikkonen L, Hirvonen J, Janne OA (2013) SUMO-1 regulates body weight and adipogenesis via PPARgamma in male and female mice. *Endocrinology* 154: 698-708
Nguea PA, Robertson J, Herrera MC, Chymkowitch P, Enserink JM (2019) Desumoylation of RNA polymerase III lies at the core of the Sumo stress response in yeast. *J Biol Chem* 294: 18784-18795
Nguyen HL, Geukens T, Maetens M, Aparicio S, Bassez A, Borg A, Brock J, Broeks A, Caldas C, Cardoso F *et al* (2023) Obesity-associated changes in molecular biology of primary breast cancer. *Nat Commun* 14: 4418
Nordsletten M, Saeed U, Myklebust T, Robsahm TE, Møller B, Skålhegg BS, Mala T, Yaqub S (2023) Body mass index and its association with 22 cancer types: a Norwegian cohort study of 481 202 cancer cases. *Acta Oncol* 62: 1273-1278
Nyman E, Bartesaghi S, Melin Rydfalk R, Eng S, Pollard C, Gennemark P, Peng X-R, Cedersund G (2017) Systems biology reveals uncoupling beyond UCP1 in human white fat-derived beige adipocytes. *npj Systems Biology and Applications* 3: 29
Ohno H, Shinoda K, Spiegelman BM, Kajimura S (2012) PPARgamma agonists induce a white-to-brown fat conversion through stabilization of PRDM16 protein. *Cell Metab* 15: 395-404
Paakinaho V, Lempiainen JK, Sigismondo G, Niskanen EA, Malinen M, Jaaskelainen T, Varjosalo M, Krijgsveld J, Palvimo JJ (2021) SUMOylation regulates the protein network and chromatin accessibility at glucocorticoid receptor-binding sites. *Nucleic Acids Res* 49: 1951-1971
Pahlavani M, Pham K, Kalupahana NS, Morovati A, Ramalingam L, Abidi H, Kiridana V, Moustaid-Moussa N (2024) Thermogenic adipose tissues: Promising therapeutic targets for metabolic diseases. *J Nutr Biochem* 137: 109832
Parreno V, Loubiere V, Schuettengruber B, Fritsch L, Rawal CC, Erokhin M, Győrffy B, Normanno D, Di Stefano M, Moreaux J *et al* (2024) Transient loss of Polycomb components induces an epigenetic cancer fate. *Nature*
Pati S, Irfan W, Jameel A, Ahmed S, Shahid RK (2023) Obesity and Cancer: A Current Overview of Epidemiology, Pathogenesis, Outcomes, and Management. *Cancers (Basel)* 15
Pei J, Zou D, Li L, Kang L, Sun M, Li X, Chen Q, Chen D, Qu B, Gao X *et al* (2024) Senp7 deficiency impairs lipid droplets maturation in white adipose tissues via Plin4 deSUMOylation. *Journal of Biological Chemistry* 300: 107319

Pruitt KD, Brown GR, Hiatt SM, Thibaud-Nissen F, Astashyn A, Ermolaeva O, Farrell CM, Hart J, Landrum MJ, McGarvey KM *et al* (2014) RefSeq: an update on mammalian reference sequences. *Nucleic Acids Res* 42: D756-763
Rauluseviciute I, Riudavets-Puig R, Blanc-Mathieu R, Castro-Mondragon JA, Ferenc K, Kumar V, Lemma RB, Lucas J, Chèneby J, Baranasic D *et al* (2024) JASPAR 2024: 20th anniversary of the open-access database of transcription factor binding profiles. *Nucleic Acids Res* 52: D174-d182
Roh HC, Tsai LTY, Shao M, Tenen D, Shen Y, Kumari M, Lyubetskaya A, Jacobs C, Dawes B, Gupta RK *et al* (2018) Warming Induces Significant Reprogramming of Beige, but Not Brown, Adipocyte Cellular Identity. *Cell Metab* 27: 1121-1137 e1125
Rosenwald M, Perdikari A, Rulicke T, Wolfrum C (2013) Bi-directional interconversion of brite and white adipocytes. *Nat Cell Biol* 15: 659-667
Rosenwald M, Wolfrum C (2014) The origin and definition of brite versus white and classical brown adipocytes. *Adipocyte* 3: 4-9
Rosonina E, Akhter A, Dou Y, Babu J, Sri Theivakadadcham VS (2017) Regulation of transcription factors by sumoylation. *Transcription* 8: 220-231
Schindelin J, Arganda-Carreras I, Frise E, Kaynig V, Longair M, Pietzsch T, Preibisch S, Rueden C, Saalfeld S, Schmid B *et al* (2012) Fiji: an open-source platform for biological-image analysis. *Nature methods* 9: 676-682
Schwalie PC, Dong H, Zachara M, Russeil J, Alpern D, Akchiche N, Caprara C, Sun W, Schlaudraff KU, Soldati G *et al* (2018) A stromal cell population that inhibits adipogenesis in mammalian fat depots. *Nature* 559: 103-108
Seeler JS, Dejean A (2017) SUMO and the robustness of cancer. *Nat Rev Cancer* 17: 184-197
Shao M, Wang QA, Song A, Vishvanath L, Busbuso NC, Scherer PE, Gupta RK (2019) Cellular Origins of Beige Fat Cells Revisited. *Diabetes* 68: 1874-1885
Shapira SN, Seale P (2019) Transcriptional Control of Brown and Beige Fat Development and Function. *Obesity (Silver Spring)* 27: 13-21
Sri Theivakadadcham VS, Bergey BG, Rosonina E (2019) Sumoylation of DNA-bound transcription factor Sko1 prevents its association with nontarget promoters. *PLoS Genet* 15: e1007991
Theurillat I, Hendriks IA, Cossec JC, Andrieux A, Nielsen ML, Dejean A (2020) Extensive SUMO Modification of Repressive Chromatin Factors Distinguishes Pluripotent from Somatic Cells. *Cell reports* 32: 108146
Turei D, Valdeolivas A, Gul L, Palacio-Escat N, Klein M, Ivanova O, Olbei M, Gabor A, Theis F, Modos D *et al* (2021) Integrated intra- and intercellular signaling knowledge for multicellular omics analysis. *Mol Syst Biol* 17: e9923
Tweedie S, Braschi B, Gray K, Jones TEM, Seal RL, Yates B, Bruford EA (2021) Genenames.org: the HGNC and VGNC resources in 2021. *Nucleic Acids Res* 49: D939-D946
Valima E, Varis V, Bureiko K, Lempiäinen JK, Schroderus AM, Oksa L, Lohi O, Kinnunen T, Varjosalo M, Niskanen EA *et al* (2025) SUMOylation inhibition potentiates the glucocorticoid receptor to program growth arrest of acute lymphoblastic leukemia cells. *Oncogene*
Wang HJ, Lee CS, Yee RSZ, Groom L, Friedman I, Babcock L, Georgiou DK, Hong J, Hanna AD, Recio J *et al* (2020) Adaptive thermogenesis enhances the life-threatening response to heat in mice with an Ryr1 mutation. *Nat Commun* 11: 5099
Wang Q, Xu C, Fan Q, Yuan H, Zhang X, Chen B, Cai R, Zhang Y, Lin M, Xu M (2021) Positive feedback between ROS and cis-axis of PIASxα/p38α-SUMOylation/MK2 facilitates gastric cancer metastasis. *Cell Death Dis* 12: 986

Xue R, Lynes MD, Dreyfuss JM, Shamsi F, Schulz TJ, Zhang H, Huang TL, Townsend KL, Li Y, Takahashi H *et al* (2015) Clonal analyses and gene profiling identify genetic biomarkers of the thermogenic potential of human brown and white preadipocytes. *Nat Med* 21: 760-768
Yu G, Wang LG, Han Y, He QY (2012) clusterProfiler: an R package for comparing biological themes among gene clusters. *OMICS* 16: 284-287
Zhao J, Qian H, An Y, Chu L, Tan D, Qin C, Sun Q, Wang Y, Qi W (2024) PPARγ and C/EBPα enable adipocyte differentiation upon inhibition of histone methyltransferase PRC2 in malignant tumors. *Journal of Biological Chemistry* 300
Zhao X, Hendriks IA, Le Gras S, Ye T, Ramos-Alonso L, Nguea PA, Lien GF, Ghasemi F, Klungland A, Jost B *et al* (2022) Waves of sumoylation support transcription dynamics during adipocyte differentiation. *Nucleic Acids Res* 50: 1351-1369
Zheng Q, Cao Y, Chen Y, Wang J, Fan Q, Huang X, Wang Y, Wang T, Wang X, Ma J *et al* (2018) Senp2 regulates adipose lipid storage by de-SUMOylation of Setdb1. *J Mol Cell Biol* 10: 258-266

Figure 1

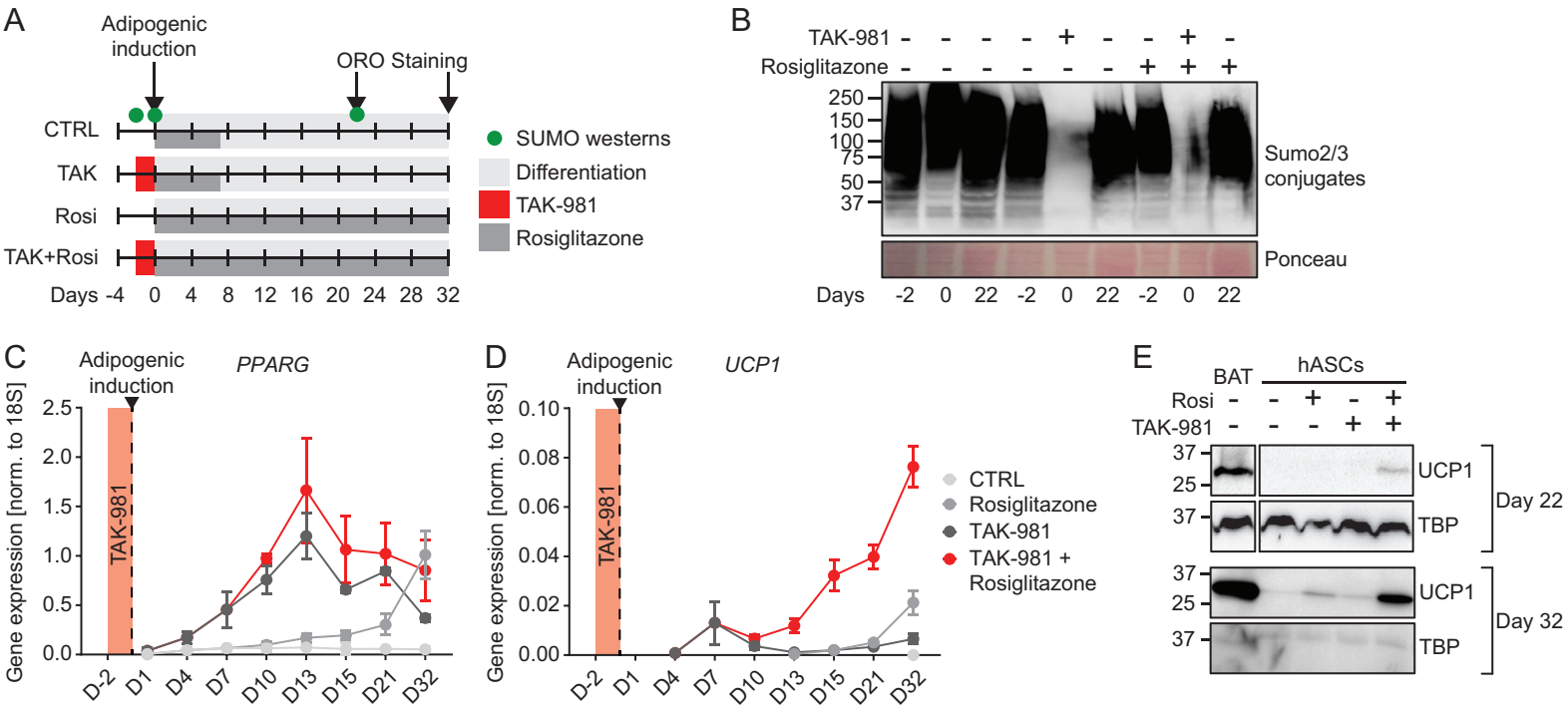
A
Adipogenic induction
ORO Staining
CTRL
TAK
Rosi
TAK+Rosi
Days -4 0 4 8 12 16 20 24 28 32
SUMO westerns
Differentiation
TAK-981
Rosiglitazone
B
TAK-981 - - - - + - - + -
Rosiglitazone - - - - - - + + +
250
150
100
75
50
37
Sumo2/3 conjugates
Ponceau
Days -2 0 22 -2 0 22 -2 0 22
C
Adipogenic induction
PPARG
Gene expression [norm. to 18S]
TAK-981
D-2 D1 D4 D7 D10 D13 D15 D21 D32
D
Adipogenic induction
UCP1
Gene expression [norm. to 18S]
TAK-981
CTRL
Rosiglitazone
TAK-981
TAK-981 + Rosiglitazone
E
BAT
hASCs
Rosi - - + - +
TAK-981 - - - + +
37
25
37
UCP1
TBP
Day 22
Day 32

Figure 2

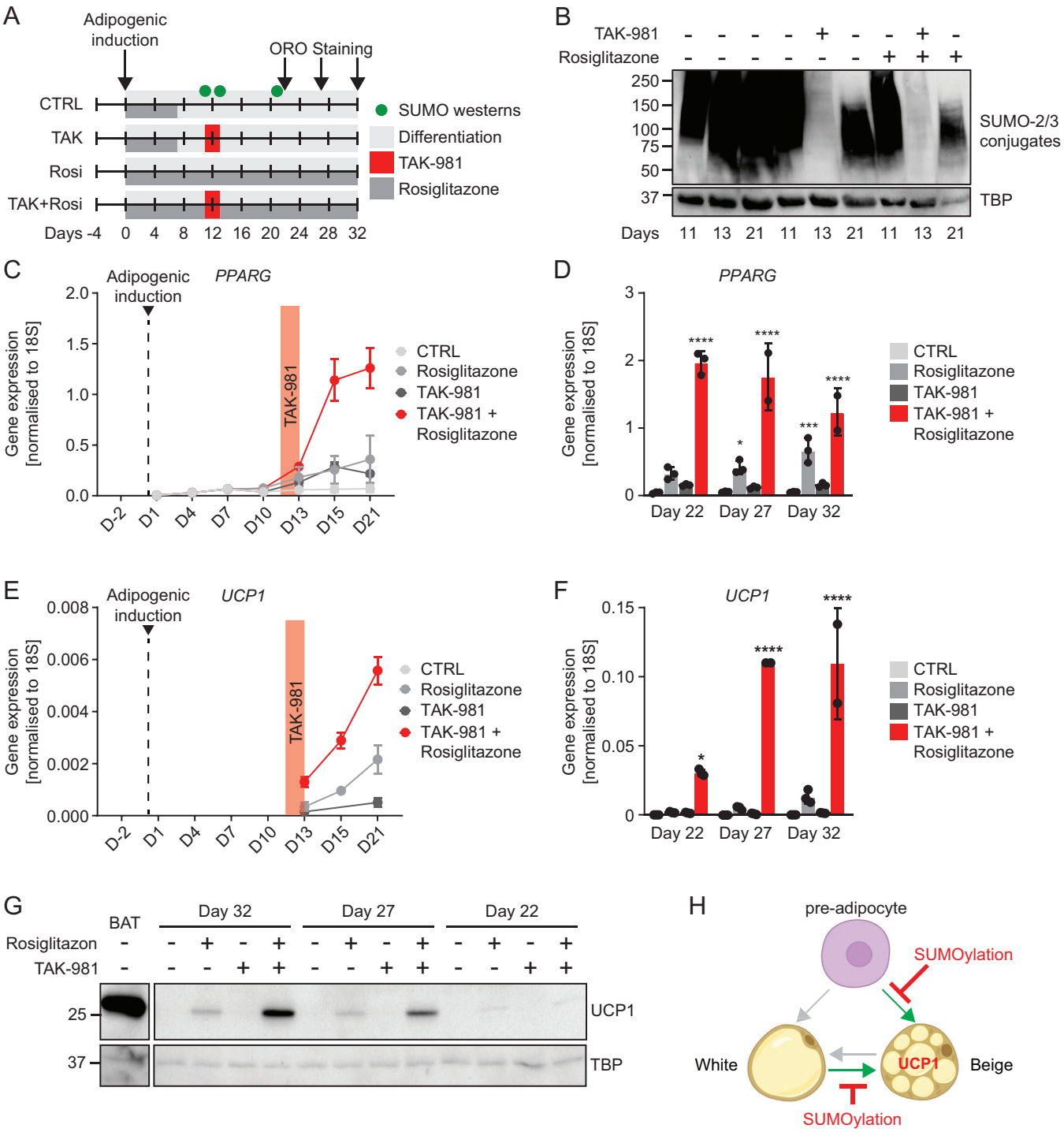
A
Adipogenic induction
ORO Staining
CTRL
TAK
Rosi
TAK+Rosi
Days -4 0 4 8 12 16 20 24 28 32
SUMO westerns
Differentiation
TAK-981
Rosiglitazone
B
TAK-981
Rosiglitazone
250
150
100
75
50
37
SUMO-2/3 conjugates
TBP
Days 11 13 21 11 13 21 11 13 21
C
Adipogenic induction
PPARG
Gene expression [normalised to 18S]
TAK-981
D-2 D1 D4 D7 D10 D13 D15 D21
CTRL
Rosiglitazone
TAK-981
TAK-981 + Rosiglitazone
D
PPARG
Day 22 Day 27 Day 32
E
Adipogenic induction
UCP1
F
UCP1
G
BAT
Day 32
Day 27
Day 22
Rosiglitazon
TAK-981
UCP1
TBP
H
pre-adipocyte
SUMOylation
White
Beige
UCP1
SUMOylation

Figure 3

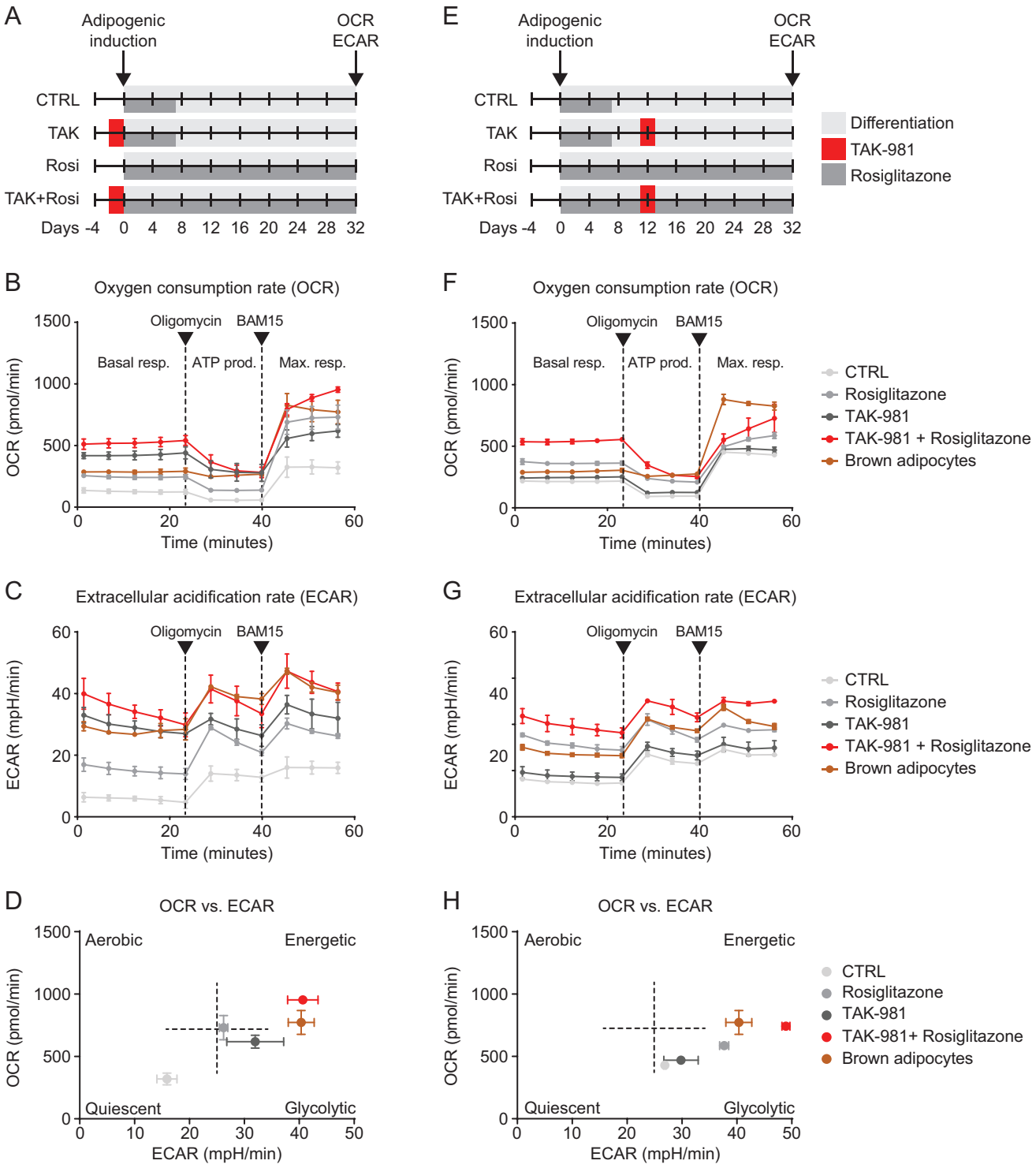
A
Adipogenic induction
OCR ECAR
CTRL
TAK
Rosi
TAK+Rosi
Days -4 0 4 8 12 16 20 24 28 32
E
Adipogenic induction
OCR ECAR
CTRL
TAK
Rosi
TAK+Rosi
Days -4 0 4 8 12 16 20 24 28 32
Differentiation
TAK-981
Rosiglitazone
B
Oxygen consumption rate (OCR)
Oligomycin
BAM15
Basal resp.
ATP prod.
Max. resp.
OCR (pmol/min)
Time (minutes)
F
Oxygen consumption rate (OCR)
Oligomycin
BAM15
Basal resp.
ATP prod.
Max. resp.
OCR (pmol/min)
Time (minutes)
CTRL
Rosiglitazone
TAK-981
TAK-981 + Rosiglitazone
Brown adipocytes
C
Extracellular acidification rate (ECAR)
Oligomycin
BAM15
ECAR (mpH/min)
Time (minutes)
G
Extracellular acidification rate (ECAR)
Oligomycin
BAM15
ECAR (mpH/min)
Time (minutes)
CTRL
Rosiglitazone
TAK-981
TAK-981 + Rosiglitazone
Brown adipocytes
D
OCR vs. ECAR
Aerobic
Energetic
Quiescent
Glycolytic
OCR (pmol/min)
ECAR (mpH/min)
H
OCR vs. ECAR
Aerobic
Energetic
Quiescent
Glycolytic
OCR (pmol/min)
ECAR (mpH/min)
CTRL
Rosiglitazone
TAK-981
TAK-981+ Rosiglitazone
Brown adipocytes

Figure 4

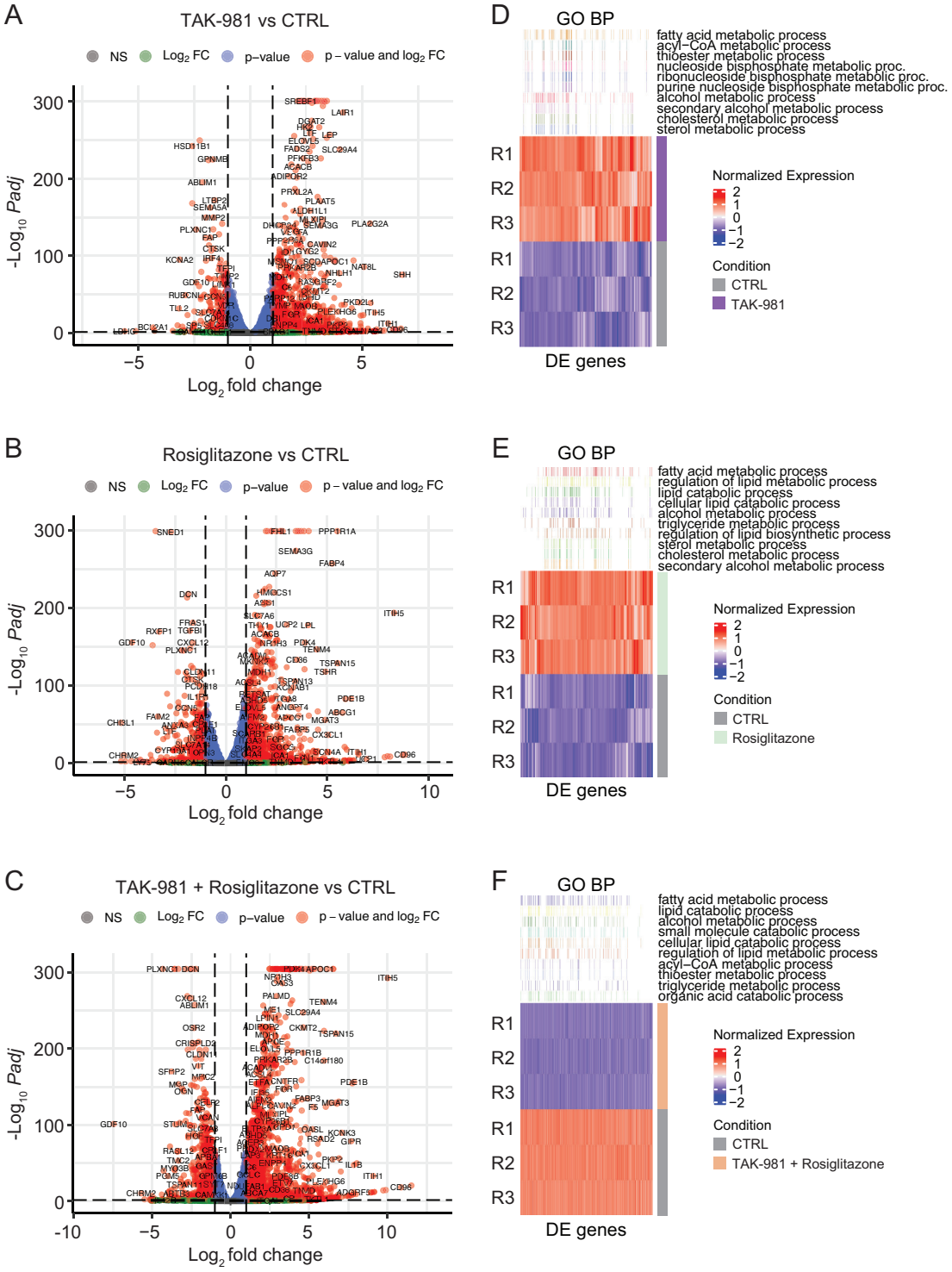
A
TAK-981 vs CTRL
NS
Log2 FC
p−value
p − value and log2 FC
-Log10 Padj
Log2 fold change
B
Rosiglitazone vs CTRL
C
TAK-981 + Rosiglitazone vs CTRL
D
GO BP
fatty acid metabolic process
acyl−CoA metabolic process
thioester metabolic process
nucleoside bisphosphate metabolic proc.
ribonucleoside bisphosphate metabolic proc.
purine nucleoside bisphosphate metabolic proc.
alcohol metabolic process
secondary alcohol metabolic process
cholesterol metabolic process
sterol metabolic process
R1
R2
R3
Normalized Expression
Condition
CTRL
TAK-981
DE genes
E
GO BP
fatty acid metabolic process
regulation of lipid metabolic process
lipid catabolic process
cellular lipid catabolic process
alcohol metabolic process
triglyceride metabolic process
regulation of lipid biosynthetic process
sterol metabolic process
cholesterol metabolic process
secondary alcohol metabolic process
Rosiglitazone
F
GO BP
fatty acid metabolic process
lipid catabolic process
alcohol metabolic process
small molecule catabolic process
cellular lipid catabolic process
regulation of lipid metabolic process
acyl−CoA metabolic process
thioester metabolic process
triglyceride metabolic process
organic acid catabolic process
TAK-981 + Rosiglitazone

Figure 5

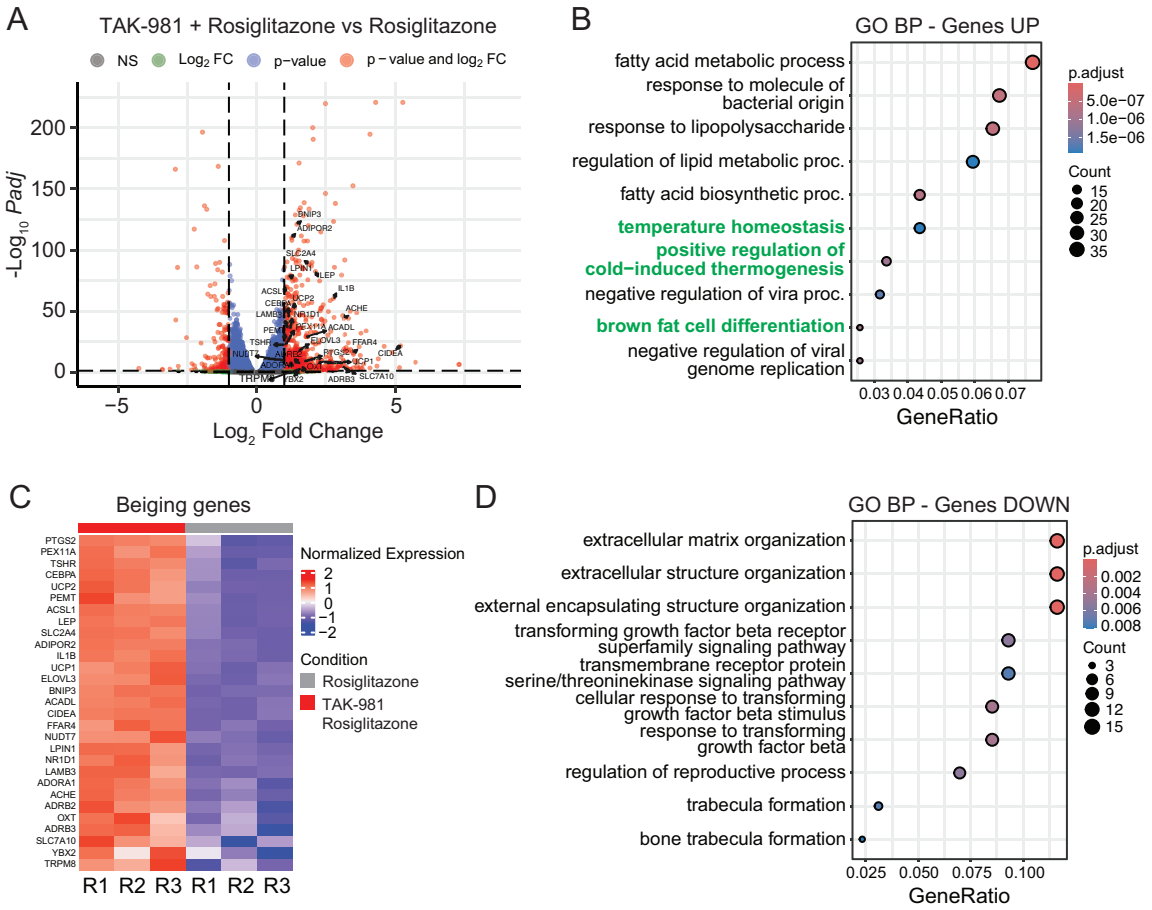
A
TAK-981 + Rosiglitazone vs Rosiglitazone
NS
Log2 FC
p−value
p − value and log2 FC
-Log10 Padj
Log2 Fold Change
B
GO BP - Genes UP
fatty acid metabolic process
response to molecule of bacterial origin
response to lipopolysaccharide
regulation of lipid metabolic proc.
fatty acid biosynthetic proc.
temperature homeostasis
positive regulation of cold−induced thermogenesis
negative regulation of vira proc.
brown fat cell differentiation
negative regulation of viral genome replication
GeneRatio
p.adjust
5.0e−07
1.0e−06
1.5e−06
Count
15
20
25
30
35
C
Beiging genes
Normalized Expression
Condition
Rosiglitazone
TAK-981
Rosiglitazone
R1 R2 R3 R1 R2 R3
D
GO BP - Genes DOWN
extracellular matrix organization
extracellular structure organization
external encapsulating structure organization
transforming growth factor beta receptor superfamily signaling pathway
transmembrane receptor protein serine/threoninekinase signaling pathway
cellular response to transforming growth factor beta stimulus
response to transforming growth factor beta
regulation of reproductive process
trabecula formation
bone trabecula formation
GeneRatio
p.adjust
0.002
0.004
0.006
0.008
Count
3
6
9
12
15

Figure 6

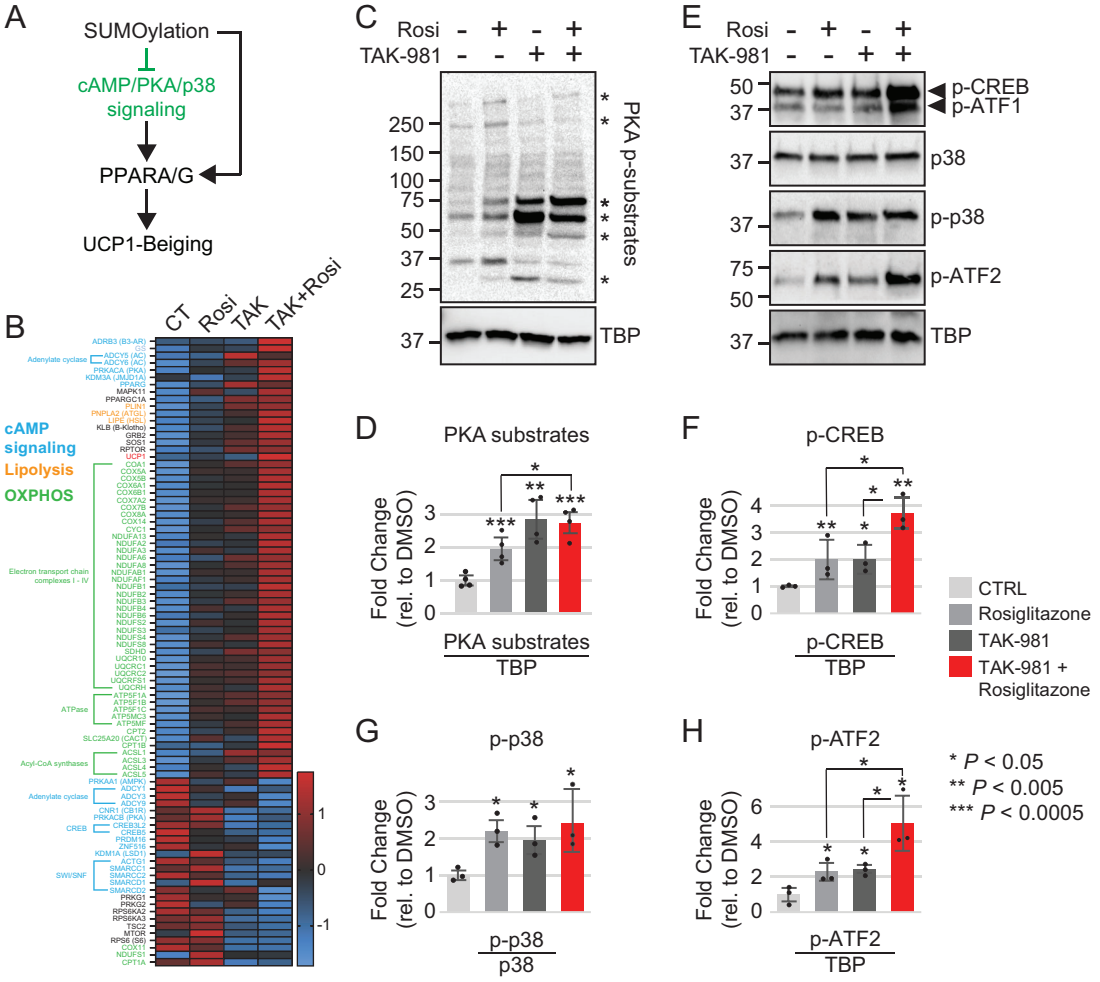
A
SUMOylation
cAMP/PKA/p38 signaling
PPARA/G
UCP1-Beiging
B
CT
Rosi
TAK
TAK+Rosi
cAMP signaling
Lipolysis
OXPHOS
C
Rosi - + - +
TAK-981 - - + +
250
150
100
75
50
37
25
PKA p-substrates
37
TBP
E
Rosi - + - +
TAK-981 - - + +
50
37
p-CREB
p-ATF1
37
p38
37
p-p38
75
50
p-ATF2
37
TBP
D
PKA substrates
Fold Change (rel. to DMSO)
PKA substrates / TBP
F
p-CREB
Fold Change (rel. to DMSO)
p-CREB / TBP
CTRL
Rosiglitazone
TAK-981
TAK-981 + Rosiglitazone
G
p-p38
Fold Change (rel. to DMSO)
p-p38 / p38
H
p-ATF2
Fold Change (rel. to DMSO)
p-ATF2 / TBP
* P < 0.05
** P < 0.005
*** P < 0.0005

Figure 7

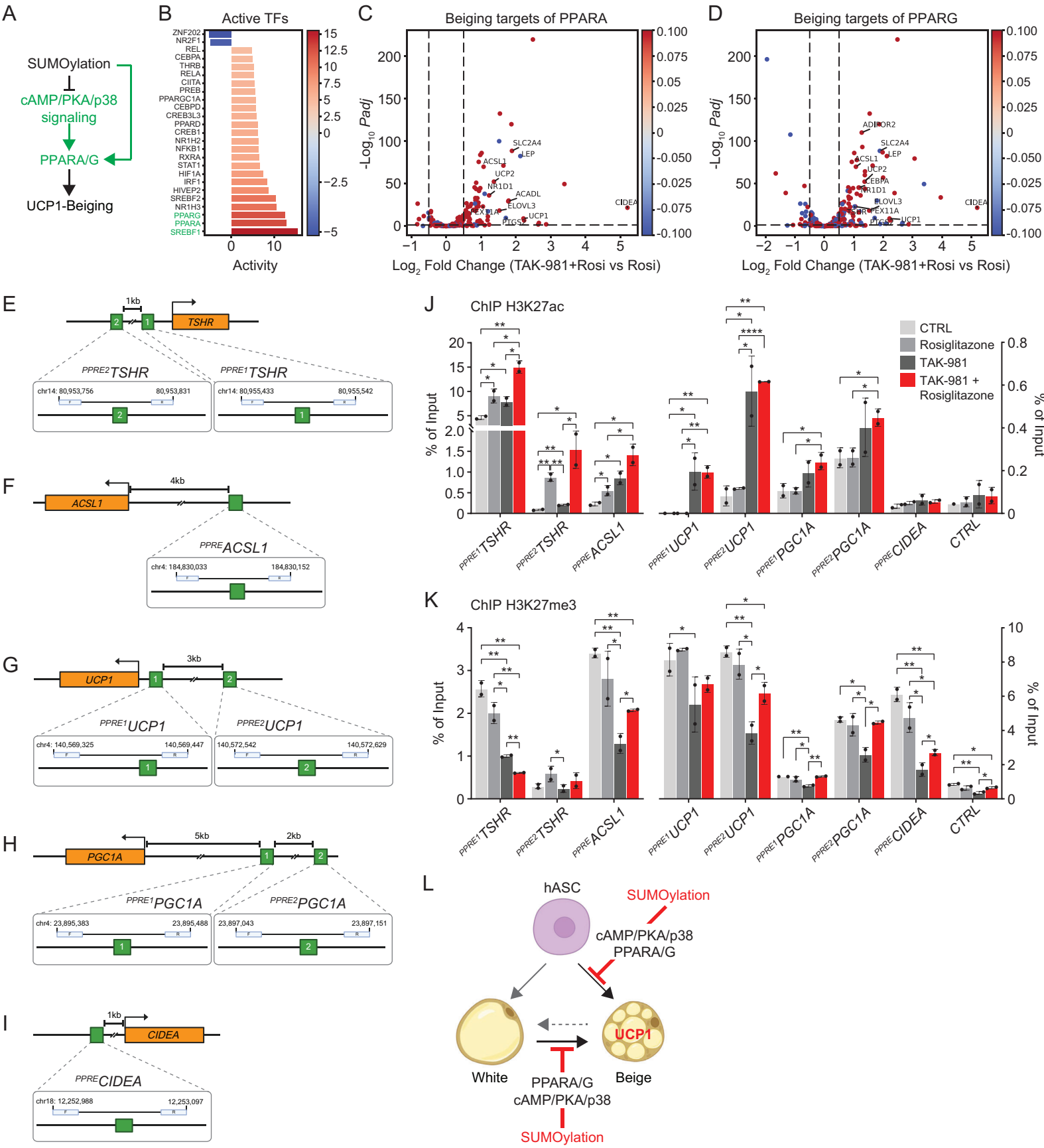
A
SUMOylation
cAMP/PKA/p38 signaling
PPARA/G
UCP1-Beiging
B
Active TFs
Activity
C
Beiging targets of PPARA
-Log10 Padj
Log2 Fold Change (TAK-981+Rosi vs Rosi)
D
Beiging targets of PPARG
-Log10 Padj
Log2 Fold Change (TAK-981+Rosi vs Rosi)
E
TSHR
PPRE2TSHR
PPRE1TSHR
F
ACSL1
PPREACSL1
G
UCP1
PPRE1UCP1
PPRE2UCP1
H
PGC1A
PPRE1PGC1A
PPRE2PGC1A
I
CIDEA
PPRECIDEA
J
ChIP H3K27ac
CTRL
Rosiglitazone
TAK-981
TAK-981 + Rosiglitazone
% of Input
K
ChIP H3K27me3
% of Input
L
hASC
SUMOylation
cAMP/PKA/p38
PPARA/G
White
Beige
UCP1
PPARA/G
cAMP/PKA/p38
SUMOylation